AN ANALYTICAL INVESTIGATION ON ELECTROOSMOTIC FLOW WITHIN A MICROCHANNEL BETWEEN TWO PARALLEL PLATES WITHOUT THE DEBYE-HUCKEL APPROXIMATION

A Thesis Submitted for Partial Fulfillment of the

Requirements for the Degree of

Master of Engineering in Mechanical Engineering

By

AVISANKHA DUTTA

[Examination Roll Number: M4MEC19008]

[Registration Number: 116475 of 2011-2012]

Under the Guidance of

Dr. SUDIP SIMLANDI

ASSOCIATE PROFESSOR

DEPARTMENT OF MECHANICAL ENGINEERING

JADAVPUR UNIVERSITY

KOLKATA – 700032

MAY 2019

Faculty of Engineering & Technology
Department of Mechanical Engineering
Jadavpur University
Kolkata-700032

Certificate of Approval*

*The foregoing thesis, entitled "**An Analytical Investigation on Electroosmotic Flow within a Microchannel between Two Parallel Plates without the Debye-Huckel Approximation**" is hereby approved as a creditable study in the area of Heat Power and Thermal Engineering carried out and presented by **Mr. Avisankha Dutta** (Registration No. 116475 of 2011 – 2012) in a satisfactory manner to warrant its acceptance as a prerequisite to the degree for which it has been submitted. It is notified to be understood that by this approval, the undersigned do not necessarily endorse or approve any statement made, opinion expressed and conclusion drawn therein but approve the thesis only for the purpose for which it has been submitted.*

Final Examination for Evaluation of the Thesis

Board of Members

_____ _____

_____ _____

***Only in case the thesis is approved**

Faculty of Engineering & Technology
Department of Mechanical Engineering
Jadavpur University
Kolkata-700032

CERTIFICATE OF RECOMMENDATION

*We hereby recommend that the thesis, entitled "**An Analytical Investigation on Electroosmotic Flow within a Microchannel between Two Parallel Plates without the Debye-Huckel Approximation**", prepared by **Mr. Avisankha Dutta** (Registration No. 116475 of 2011-2012) a student of ME second year, has been evaluated by us & found satisfactory. It is therefore, being accepted in partial fulfillment of the requirement of awarding the degree of Master of Engineering in Mechanical Engineering with specialization in Heat Power engineering.*

Dr. Sudip Simlandi
Associate Professor
Department of Mechanical Engineering
Jadavpur University
Kolkata-700032

Countersigned by –

Prof. Gautam Majumdar
Head of the Department
Department of Mechanical Engineering
Jadavpur University
Kolkata-700032

Prof. Chiranjib Bhattacharjee
Dean
Faculty of Engineering & Technology
Jadavpur University
Kolkata-700032

DECLARATION OF ORIGINALITY AND COMPLIANCE OF ACADEMIC ETHICS

I hereby declare that the thesis contains literature survey and original research work by the undersigned candidate, as a part of his MASTER OF ENGINEERING IN MECHANICAL ENGINEERING studies. All information in this document have been obtained and presented in accordance with the academic rules and ethical conduct.

I also declare that, as required by these rules of conduct, I have fully cited and referenced all the material and results that are not original to this work.

Name: AVISANKHA DUTTA

Examination Roll Number: M4MEC19008

Class Roll Number: 001711202003

University Registration No: 116475 of 2011-12

Thesis Title: *AN ANALYTICAL INVESTIGATION ON ELECTROOSMOTIC FLOW WITHIN A MICROCHANNEL BETWEEN TWO PARALLEL PLATES WITHOUT THE DEBYE-HUCKEL APPROXIMATION*

Signature with Date:

Table of Contents

Acknowledgement

*I owe a deep sense of gratitude to my respected thesis advisor **Dr. Sudip Simlandi** for his esteemed guidance and encouragement throughout this work. Without his generous support and motivation this would not have been completed. It was a great privilege and experience to work under him.*

*I am indebted to **Prof. Gautam Majumdar** (present Head) and **Prof. Dipankar Sanyal** (Former Head) Mechanical Engineering Department, Jadavpur University for providing the facilities during the course of investigation.*

I am also grateful to all the faculty members of Mechanical Engineering Department, Jadavpur University and Research Scholars of Mechanical Engineering Department, Jadavpur University for their moral support, help and cooperation. In this regard, I also thank all the faculty members of Mechanical Engineering Department for their constant support.

Thanks to all my friends who helped me with their valuable suggestions. I want to convey my heartiest gratitude to all my batch mates and junior friends for kind cooperation and making my two years at Jadavpur University memorable.

Finally, I thank my parents for being a source of continuous moral courage and inspiration.

Date:

_____

Avisankha Dutta

Registration No: 116475 of 2011-12

Examination Roll No: M4MEC19008

Abstract

In the present work, an electroosmotic flow of a Newtonian liquid within a microchannel between two parallel plates has been studied analytically. Electroosmotic flow is an important area of research because of its widespread applications in biomedical and chemical industries. The present study has been divided into three sections. Firstly, an electroosmotic flow between two parallel plates with no-slip boundary conditions is considered. The Debye-Huckel linear approximation is ignored to minimize error in results. The electrical potential distribution is represented by the non-linear Poisson-Boltzmann equation which is solved adopting homotopy perturbation method (HPM) without the Debye-Huckel approximation to obtain electrical potential field. Subsequently, the Navier-Stokes equation has been modified and solved analytically using the potential field to determine the velocity distribution. The energy equation has also been modified using scale analysis and solved analytically incorporating the velocity profile obtained to get the temperature profile. Finally, an expression of Nusselt number is determined based on the velocity and temperature profiles. The proposed results (without the Debye-Huckel approximation) are presented in a comparative way with the FDM and an existing conventional method with the Debye-Huckel approximation to compare the accuracy level of the proposed method. It is observed that the proposed results show good agreement with the numerical results for a wide range of wall zeta potential whereas the exiting conventional method shows deviation from the numerical results for higher value of zeta potential. Finally, Nusselt number is predicted with the electrokinetic length for different values zeta potential. It is observed that the present analysis may be used for prediction of electroosmotic flow within microchannels for a wide range of wall zeta potential.

In the second section, an analytical solution is presented for a combined pressure driven electroosmotic flow of a Newtonian liquid within a microchannel between two parallel plates. The electroosmotic flow is considered to be induced by an externally applied electrostatic potential field and a pressure gradient. The no-slip boundary conditions are considered. The reduced form of the Navier-Stokes and the energy equations are considered, respectively to determine velocity and temperature distributions. The electrical potential distribution is determined using HPM without the Debye-Huckel linear approximation. The Navier-Stokes and the energy equations

subjected to respective boundary conditions are solved analytically. The results obtained are validated with existing literature and show good agreement. An expression of C_f Re product is obtained from the velocity field. The zeta potential is varied for a particular electrokinetic length and proposed results are presented graphically. Finally, the Nusselt number is presented with electrokinetic length for different values of zeta potential. The results demonstrate the influence of the zeta potential on the electrical potential, velocity, temperature distributions, C_f Re product and Nusselt number.

In the third section, an analytical investigation has been conducted on a combined pressure driven electroosmotic flow of a Newtonian liquid within a microchannel between two parallel plates. The flow is considered with first order slip boundary conditions. The non-linear Poisson-Boltzmann equation without the Debye-Huckel linear approximation is used to determine the electric potential distribution. The reduced form of the Navier-Stokes equation with slip boundary conditions is considered to determine velocity field and skin friction coefficient, whereas the energy equation is simplified to obtain temperature distribution, Nusselt number and entropy generation rates. The homotopy perturbation method (HPM) is adopted as an analytical tool to solve the Poisson-Boltzmann equation while, the Navier-Stokes and energy equations are solved analytically to obtain the velocity and temperature distributions. The results obtained are validated with existing literature and show good agreement. Proposed results for potential, velocity and temperature fields are presented graphically varying wall zeta potential, slip coefficient and pressure gradient. Subsequently, a parametric study is carried out for the skin friction coefficient and the Nusselt number. Finally, an effort is made to determine local volumetric entropy generation rate and global entropy generation rate. The results demonstrate the effect of pressure gradient and the Brinkmann number on the entropy generation rates.

List of Figures

Nomenclature

Symbol	Description
$2H$	Distance between two parallel plates in Chapter 1 and 2 (m)
H	Distance between two parallel plates in Chapter 3 (m)
Y	Perpendicular distance of a given point from the centre (m)
n_0	Bulk ionic concentration (m^{-3})
z	Valence of ions
e	Electric charge (C)
k_b	Boltzmann constant (JK^{-1})
T	Absolute temperature (K)
Z	Non-dimensional zeta potential
u	Velocity in x-direction (ms^{-1})
u_m	Mean velocity (ms^{-1})
U	Non-dimensional velocity
F_x	Electrical force per unit volume of the liquid (Nm^{-3})
E_x	Electric field strength (Vm^{-1})
E	Non-dimensional electric field strength
L	Distance between the two electrodes (m)
$C_1, \Delta P$	Non-dimensional pressure gradient
C_2	Ratio of the electrical force to the frictional force per unit volume
B	Slip coefficient
q_w	Heat flux at wall (Wm^{-2})
C_f	Skin friction coefficient
c_p	Specific heat ($Jkg^{-1}K^{-1}$)
T_w	Wall temperature (K)
T_m	Mean temperature (K)
Nu	Nusselt number
S_G	Local volumetric entropy generation rate ($JK^{-1}s^{-1}$)

S_{total}	Non-dimensional global entropy generation rate

Greek symbols

ψ	Electric potential due to EDL (V)
Ψ	Non-dimensional electric potential
ε	Dielectric constant of the electrolyte solution ($Cm^{-1}V^{-1}$)
ξ	Zeta potential at the wall (V)
κ	Inverse Debye-Huckle length (m^{-1})
λ	electrokinetic length (m)
μ	dynamic viscosity (Pa s)
β	Slip coefficient (m)
ρ_f	Local net charge density (Cm^{-3})
τ_w	Shear stress at wall (MPa)
ρ	Density (kgm^{-1})
Φ	Non-dimensional temperature
θ	Non-dimensional temperature at wall

Subscripts

m	Mean
x	Along *x*-direction
w	At the wall
H	Entropy generation rate due to heat diffusion
J	Entropy generation rate due to Joule heating
V	Entropy generation rate due to viscous dissipation

1. Introduction

In recent days, the study on microfluidic systems has become an important area of research for various potential applications in biomedical and chemical industries. Biomedical micro-electro-mechanical systems (bioMEMS) or lab-on-a-chip devices can perform sample injection, chemical reaction, separation, and detection in a single integrated microfluidic circuit [1, 2]. The important microfluidic operations in various bioMEMS are pumping, mixing, thermal cycling, dispensing and separating. Various techniques such as thermopneumatic, magnetohydrodynamic, piezoelectric, electrostatic, and electroosmotic pumping have been proposed for fluid delivery [3-6]. Among them, electroosmotic pumping is favoured for fluid delivery through micro-devices because of the absence of moving parts and pulsating flows, ease of microfabrication, valve-less switching and great degree of flow control. Electroosmotic pumping is based on electroosmotic flow (EOF) within microchannels. It is important to understand the fundamental characteristics of EOF within microchannels for optimal design of electroosmotic pumps. When an electrolytic solution is under no flow condition, the ions dissociate. Those ions having charge opposite to that of the surface are attracted by the surface while, the ions having similar charge stay away from the surface. Thus, two layers of positively and negatively charged ions are formed near the surface which are called electric double layer (EDL) [5-10]. If a pressure gradient or an electric field or both are applied tangentially along such a charged surface, the ions in the diffuse layer will start moving under the action of a body force exerted by the pressure field or electric field, resulting in a simple EOF or a combined pressure driven EOF [16, 22-26]. The nature of EOF depends on the interactions between the fluid and the surface properties of the solid wall. Therefore, for an efficient control of the electroosmotic pumping, a detailed and systematic knowledge on the liquid flow behaviour is essential.

2. Literature survey

In this section, existing literatures based on EOF are studied. Firstly, the papers based on development of EOF are studied. Next, literatures presenting solution methods have been studied. Finally, studies on pressure driven EOF with slip boundary conditions are considered.

- Burgreen and Nakache [12] studied the effect of the surface potential on liquid

transport through ultrafine capillary slits under an imposed electrical field. Debye-Huckel linear approximation was followed for finding the electrical potential distribution.

- Jooybari and Chen [13] derived analytical solutions for electrical potential distribution within an interstitial EDL in various particle geometries. An exact analytical solution of the Poisson-Boltzmann equation was obtained for slab-shaped particles containing an electrolyte solution.
- Masood Khan et al. [14] discussed the dynamics of an EOF in cylindrical domain. The linearized Poisson–Boltzmann equation and the Cauchy momentum equation were solved using the temporal Fourier and finite Hankel transforms.
- Yang and Li [16] used a finite difference scheme to study the electrokinetic effects of pressure-driven flow in rectangular microchannels. In his study, Yang used the Green's function method to analytically solve the dynamic electroosmotic flow field.
- Min et al. [18] analytically solved the fundamental characteristics of electroosmotic flow through rectangular pumping channels without the Debye-Huckel approximation. The Poisson–Boltzmann equation for the electric potential distribution and the momentum equation for the velocity profile are solved by averaging method.
- Tunc and Bayazitoglu [19] analyzed the convection heat transfer for a hydrodynamically and thermally fully developed slip flow in a rectangular microchannel. The velocity and temperature profiles were determined by integral transform technique and the values of Nusselt number were presented for different aspect ratios.
- Mala et al. [20] studied the effects of the EDL field and channel size on the velocity distribution, streaming potential, apparent viscosity, temperature distribution and heat transfer coefficient for a flow through a microchannel between two parallel plates at constant and equal temperatures.
- Jain and Jensen [21] presented an analytical investigation on the effects of electrostatic potential in microchannels. The energy equation was solved with the Nusselt number for constant wall heat flux and constant wall temperature boundary conditions and they were presented with analytic expressions over a wide range of operating conditions.

- Ngoma and Erchiqui [22] presented a study on incompressible liquid exhibiting hydrodynamically and thermally steady fully developed laminar flow with the slip boundary condition through a microchannel between two parallel plates with imposed heat flux. They considered the combined effect of pressure-driven flow and electro-osmosis. The Poisson–Boltzmann, the modified Navier–Stokes and the energy equations were solved to obtain the electric potential, flow, and thermal characteristics.
- Shamshiri et al. [24] performed the first and second law analysis for a combined pressure-driven and electroosmotic flow of non-Newtonian liquid through a uniform microannulus. The governing equations are solved numerically in cylindrical polar coordinates using finite difference method. In the second law analysis, the entropy generation rates were determined and the influence of thermal diffusion, Joule heating and viscous dissipation are examined on the total entropy generation.
- Wang and Jian [25] investigated the thermal transport properties of fluid through slit soft nanochannels under the combined influences of pressure-driven and streaming potential. The non-dimensional temperature distribution was analytically determined from the energy equation based on the electric potential and velocity distributions. Finally, the entropy generation rates are obtained and presented graphically.
- Jing et al. [26] developed closed form expressions of Joule heating, viscous dissipation and Nusselt number for steady, laminar, hydrodynamically and thermally fully developed pressure driven EOF with charge-dependent slip in a microchannel. The effects of zeta potential on the Joule heating, viscous dissipation and Nusselt number were analyzed.

3. Summary of literature survey

In the existing literature, the following observations were made

- The analytical solution describing the electrical potential distribution is obtained from the assumption that the electric potential approaches zero at the center of the channel.
- If the channel width is extremely small and comparable to the EDL thickness, the

electrical potential at the center approaches a non-zero value and the assumption in the existing studies may be invalid.

- The electrical potential distribution within a microchannel is determined by a simplified analysis based on the Debye-Huckel linear approximation which is valid only when the wall zeta potential is very small (usually <25 mV) [18].
- Higher values of zeta potential (100–200mV) are frequently encountered in practical applications [18]. As a result, the accuracy level of the result is reduced. For such instances, in place of the Debye-Huckel approximation tedious and time-consuming numerical simulations are used.
- The existing analytical methods applied are complex, lengthy and laborious.

Hence, it is highly desirable to use a simple analytical method to predict the fundamental characteristics of EOF within microchannels without the Debye-Huckel approximation.

4. Work plan

In the present work, homotopy perturbation method (HPM) is considered as an analytical tool to solve the Poisson-Boltzmann equation as it is a simple and powerful solving technique. Subsequently, the electric potential distribution obtained is used to analytically solve the Navier-Stokes and the energy equations for determination of velocity and temperature distributions, respectively, for an EOF within a microchannel between two parallel plates.

The present study on EOF is categorized into three sections as follows

- EOF within a microchannel between two parallel plates with no-slip boundary conditions.
- Combined pressure driven EOF within a microchannel between two parallel plates with no-slip boundary conditions.
- Combined pressure driven EOF within a microchannel between two parallel plates with first order slip boundary conditions.

CHAPTER 1

In this segment, an EOF within a microchannel between two parallel plates with no-slip boundary conditions is considered. The HPM is adopted to solve the non-linear Poisson-Boltzmann equation without the Debye-Huckel linear approximation to get the electrical potential distribution. The result obtained is used to analytically solve the Navier-Stokes equation and the energy equation for determination of velocity and temperature distributions, respectively. The results obtained by the proposed method are compared with an existing conventional method based on the Debye-Huckel approximation and a numerical method. Finally, Nusselt number is presented as a function of electrokinetic length for different values zeta potential.

5. Description of physical problem

The present study considers a microchannel consisting of two parallel plates separated by a distance 2H as shown in Fig. 1. The plates extend to infinity in the *x* and *z*-directions. Due to the symmetry in the potential and velocity fields, the solution domain is reduced to a half section of the channel (the hatched area). Two plate type electrodes are placed apart by length L normal to the parallel plates such that an electric field is induced in the *x*-direction.

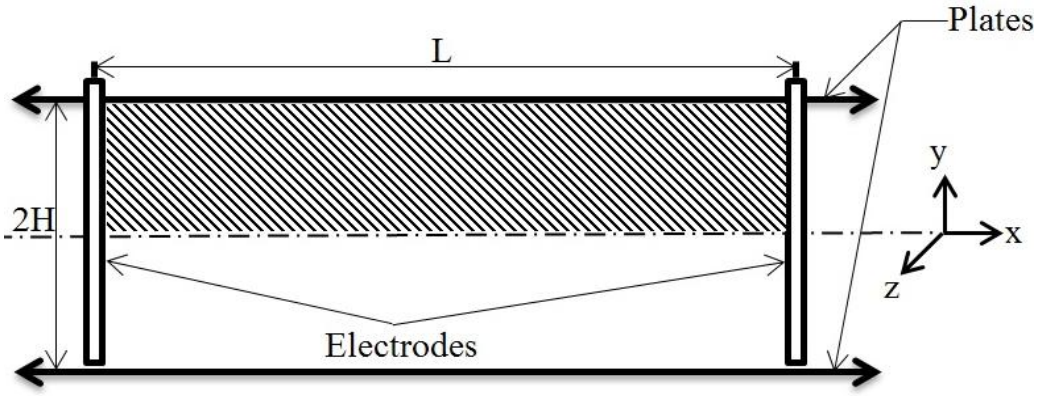

Fig. l: Schematic of the parallel plate microchannel

The following assumptions are considered in the present analysis

- The liquid is an incompressible, Newtonian and symmetric electrolyte.
- The thermophysical properties are constant.
- The flow is steady, laminar, hydrodynamically and thermally fully developed.
- No-slip boundary conditions and no wall temperature jump are considered.

6. Mathematical formulation

In the present study, an electroosmotic flow through a microchannel between two parallel plates is considered. The constitutive governing equations are written as

6.1 Poisson-Boltzmann equation

The one dimensional EDL field can be described by the Poisson-Boltzmann equation as [15, 17, 18]

$$\partial^2\psi/\partial y^2 = (2zen_0/\varepsilon)\sinh(ze\psi/k_bT) \tag{1}$$

The boundary conditions are stated as

at $y = 0$, $\partial\psi/\partial y = 0$ and at $y = H$, $\psi = \xi$

6.2 Momentum equation

The Navier-Stokes equation along the *x*-axis is considered by a balance between the shear stresses in the fluid and externally imposed electric field force as [15, 17, 18]

$$\mu(\partial^2 u/\partial y^2) + F_x = 0 \tag{2}$$

where, $F_x = \rho_f E_x$

Therefore, the Eq. (2) can be written as

$$\mu(\partial^2 u/\partial y^2) + \rho_f E_x = 0 \tag{3}$$

The boundary conditions are

at $y = 0$, $\partial u/\partial y = 0$ and at $y = H$, $u = 0$

6.3 Energy equation

The energy equation for a steady fully developed laminar liquid flow is given as [15, 17, 18]

$$u(\partial T/\partial x) = \alpha(\partial^2 T/\partial y^2) \tag{4}$$

where, $\alpha = \rho C_p/\mu$

The boundary conditions are given as

at $y = 0$, $\partial T/\partial y = 0$ and at $y = H$, $T = T_w$

7. Solution method

As stated before, one of the objectives of the present work is to provide a simple, less laborious analytical solution apart from the analysis of EOF between two parallel plates. The homotopy perturbation method (HPM) is adopted in the present analysis. Thus, the Poisson-Boltzmann equation is solved using HPM and the constitutive governing equations for velocity and temperature distributions have been solved analytically using the potential distribution obtained by HPM.

7.1 Electric potential distribution

The Eq. (1) and its boundary conditions are non-dimensionalized by introducing the dimensionless variables such as

$$\mathrm{Y} = y/H\,,\ \Psi = ze\psi/(k_bT)\,,\ Z = 2ze\xi/(k_bT)$$

The non-dimensional form of Eq. (1) becomes

$$\partial^2\Psi/\partial\mathrm{Y}^2 = \lambda^2 \sinh\Psi \tag{5}$$

where $\lambda = \kappa H$ and $\kappa = \sqrt{[2z^2e^2n_0/(\varepsilon k_bT)]}$

The corresponding non-dimensional boundary conditions are

at $\mathrm{Y}=0$, $\partial\Psi/\partial\mathrm{Y}=0$ and at $\mathrm{Y}=1$, $\Psi = Z$

It is already stated that most of the existing works on EOF considered the Debye-Huckel approximation where $\sinh\Psi$ in Eq. (5) has been taken as Ψ. As a result, accuracy level of results may reduce. Again, for higher wall zeta potential, the deviation in result is more. Hence, in the present work, the Debye-Huckel approximation is ignored and $\sinh\Psi$ is expanded based on the Taylor series of expansion as

$$\sinh\Psi = \Psi + \Psi^3/3! + \cdots \tag{6}$$

Substituting the above relation in Eq. (5) yields

$$\partial^2\Psi/\partial Y^2 = \lambda^2(\Psi + \Psi^3/3! + \cdots) \tag{7}$$

The Eq. (7) is solved by constructing a homotopy as

$$\Psi'' - \omega^2\Psi + p[(\lambda^2 - \omega^2)\Psi + \lambda^2\Psi^2/3] = 0 \tag{8}$$

where, $\Psi'' = \partial^2\Psi/\partial\mathrm{Y}^2$, ω is a modified inverse Debye length and $p \in [0,1]$ is an embedding parameter.

The power series in p used to find the solution of Eq. (8) is

$$\Psi = \Psi_0 + p\Psi_1 + p^2\Psi_2 + \cdots \tag{9}$$

Substituting the above expression in Eq. (8) and arranging the coefficients of p powers, one can obtain

$$p^0\left(\Psi_0'' - \omega^2\Psi_0\right) + p^1[\Psi_1'' - \omega^2\Psi_1 - \left(\lambda^2 - \omega^2\right)\Psi_0 - \lambda^2\Psi_0^3/3!] = 0 \tag{10}$$

Equating the coefficients of p^0, p^1 to zero gives

$$p^0: \quad \Psi_0'' - \omega^2\Psi_0 = 0 \tag{11}$$

$$p^1: \quad \Psi_1'' - \omega^2\Psi_1 - \left(\lambda^2 - \omega^2\right)\Psi_0 - \lambda^2\Psi_0^3/3! = 0 \tag{12}$$

The Eq. (11) is solved using the boundary conditions

$$\Psi_0(1) = Z, \ \Psi_0'(0) = 0$$

resulting in

$$\Psi_0 = Z\cosh(\omega Y)/\cosh(\omega) \tag{13}$$

Substituting the above expression in Eq. (12) and simplifying the equation gives

$$\Psi_1'' - \omega^2\Psi_1 - (\lambda^2 - \omega^2)Z\cosh(\omega Y)/\cosh(\omega) - \lambda^2 Z^3[3\cosh(\omega Y) + \\ + \cosh(3\omega Y)]/[24\cosh^3(\omega)] = 0 \tag{14}$$

In order to eliminate cosh(ωY) from Eq. (14) the coefficients are collected and equated to zero as

$$(\lambda^2 - \omega^2)Z/\cosh(\omega) + \lambda^2 Z^3/[8\cosh^3(\omega)] = 0$$

to give the value of ω as

$$\omega = \sqrt{[(8\lambda^2 - 8) + \sqrt{64\lambda^4 + 128\lambda^2 + 32\lambda^2 Z^2 + 64}]/16} \tag{15}$$

Eliminating $\cosh(\omega Y)$ the Eq. (14) becomes

$$\Psi_1'' - \omega^2\Psi_1 - \lambda^2 Z^3\cosh(3\omega Y)/[24\cosh^3(\omega)] = 0 \tag{16}$$

Now applying the boundary conditions

$$\Psi_1(1) = 0, \ \Psi_1'(0) = 0$$

the Eq. (16) is solved as

$$\Psi_1 = [\lambda^2 Z^3/192\omega^2\cosh^3(\omega)][\cosh(3\omega Y) - \cosh(3\omega)\cosh(\omega Y)/\cosh(\omega)] \tag{17}$$

Substituting the results of Eq. (13) and Eq. (17) in Eq. (9) and considering $p = 1$, the electrical potential distribution is obtained as

$$\Psi = A_1\cosh(\omega Y) + A_2\cosh(3\omega Y) \tag{18}$$

where, $A_1 = Z/\cosh(\omega) - \lambda^2 Z^3\cosh(3\omega)/[192\omega^2\cosh^4(\omega)]$ and $A_2 = \lambda^2 Z^3/[192\omega^2\cosh^3(\omega)]$

7.2 Velocity distribution

The electrical potential distribution obtained in Eq. (18) is used to determine velocity profile. The Eq. (3) can be rewritten as

$$\mu(\partial^2 u/\partial y^2) = \varepsilon E_x \partial^2 \psi/\partial y^2 \tag{19}$$

where $\rho_f = -\varepsilon \partial^2 \psi/\partial y^2$

The Eq. (19) is non-dimensionalized incorporating the following non-dimensional terms

$U = u/u_m,\ E = E_x L/\xi,\ M = 2zen_0 \xi H^2/(\mu u_0 L)$

Hence, the non-dimensional velocity field is written as

$$\partial^2 U/\partial \mathrm{Y}^2 = (ME/\lambda^2)(\partial^2 \Psi/\partial \mathrm{Y}^2) \tag{20}$$

The corresponding non-dimensional boundary conditions become,

at $\mathrm{Y} = 0, \partial U/\partial \mathrm{Y} = 0$ and at $\mathrm{Y} = 1,\ U = 0$

Integrating Eq. (20) twice with respect to Y with the given boundary conditions, the velocity profile is obtained as

$$U = (MEZ/\lambda^2)[\{\mathrm{A}_1 \cosh(\omega \mathrm{Y}) + \mathrm{A}_2 \cosh(3\omega \mathrm{Y})\}/Z - 1] \tag{21}$$

The expression of (MEZ/λ^2) is determined from the definition of mean velocity as

$$\int_0^1 U dY = 1 \tag{22}$$

and obtained as

$$(MEZ/\lambda^2) = 1/[\{\mathrm{A}_1 \sinh(\omega)/(\omega) + \mathrm{A}_2 \sinh(3\omega)/(3\omega)\}/Z - 1] \tag{23}$$

Finally, the velocity field is represented as

$$U = \frac{[\{\mathrm{A}_1 \cosh(\omega \mathrm{Y}) + \mathrm{A}_2 \cosh(3\omega \mathrm{Y})\}/Z - 1]}{[\{\mathrm{A}_1 \sinh(\omega)/(\omega) + \mathrm{A}_2 \sinh(3\omega)/(3\omega)\}/Z - 1]} \tag{24}$$

7.3 Temperature distribution

In this section an effort is made to determine temperature profile using the velocity profile obtained. Hence, the Eq. (4) for temperature field is simplified by performing scale analysis as

$\dot{q}_w'' \sim (\dot{m} c_p \Delta T/A) \sim \rho c_p u_m \Delta T$ and $\dot{q}_w'' \sim h(T_m - T_w)$

From the above relations it is observed that

$$\partial T/\partial x = \Delta T/\Delta x = \dot{q}_w''/(\rho u_m c_p H) \tag{25}$$

Combining Eq. (4) and Eq. (25) the relation obtained is as follows

$$\partial^2 T / \partial y^2 = u\dot{q}''_w / (\alpha \rho u_m c_p H) \tag{26}$$

The Eq. (26) is non-dimensionalized considering

$\Phi = (T - T_w)/(T_m - T_w)$ and $Nu = (4H)(h)/K$

and is rewritten as

$$\partial^2 \Phi / \partial \mathrm{Y}^2 = (Nu)(U)/4 \tag{27}$$

The corresponding boundary conditions become

at $\mathrm{Y} = 0$, $\partial\Phi/\partial\mathrm{Y} = 0$ and at $\mathrm{Y} = 1$, $\Phi = 0$

Substituting Eq. (24) in Eq. (27) gives

$$\partial^2 \Phi / \partial \mathrm{Y}^2 = (NuMEZ/4\lambda^2)[\{\mathrm{A}_1 \cosh(\omega \mathrm{Y}) + \mathrm{A}_2 \cosh(3\omega \mathrm{Y})\}/Z - 1] \tag{28}$$

The Eq. (28) is integrated twice with respect to Y with the given boundary conditions to obtain temperature profile as

$$\begin{aligned}\Phi = (NuMEZ/4\lambda^2)[[9\mathrm{A}_1\{\cosh(\omega \mathrm{Y}) - \cosh(\omega)\} + \\ + \mathrm{A}_2\{\cosh(3\omega \mathrm{Y}) - \cosh(3\omega)\}]/(9Z\omega^2) + (1 - Y^2)/2]\end{aligned} \tag{29}$$

Finally, to determine Nusselt number, the mean temperature is expressed as

$$\int_0^1 U\Phi dY = 1 \tag{30}$$

The expression for Nusselt number is obtained at the solid wall as

$$\begin{aligned}Nu = \frac{4[\{3\mathrm{A}_1 \sinh(\omega \mathrm{Y}) + \mathrm{A}_2 \sinh(3\omega \mathrm{Y})\}/(3Z\omega) - 1]^2}{[\mathrm{A}_1^2\{1/2 - \sinh(2\omega)/(4\omega)\}/(Z^2\omega^2) + \mathrm{A}_1\mathrm{A}_2\{5\sinh(2\omega)/(6\omega) + \\ - 5\sinh(4\omega)/(12\omega)\}/(9Z^2\omega^2) + \mathrm{A}_2^2\{1/2 - \sinh(6\omega)/(12\omega)\}/(9Z^2\omega^2) + \\ + 2\mathrm{A}_1\{\cosh(\omega)/(\omega^2) - \sinh(\omega)/(\omega^3)\}/(Z) + 2\mathrm{A}_2\{\cosh(3\omega)/(9\omega^2) + \\ - \sinh(3\omega)/(27\omega^3)\}/(Z) - 1/3]\end{aligned} \tag{31}$$

8. Result and discussion

Finally, a Matlab program is developed to predict electrical potential, velocity and temperature distributions. The proposed method (without the Debye-Huckel approximation) is presented in a comparative way with a numerical method (FDM) and the existing conventional method [17] based on the Debye-Huckel approximation to compare the accuracy level of the proposed method.

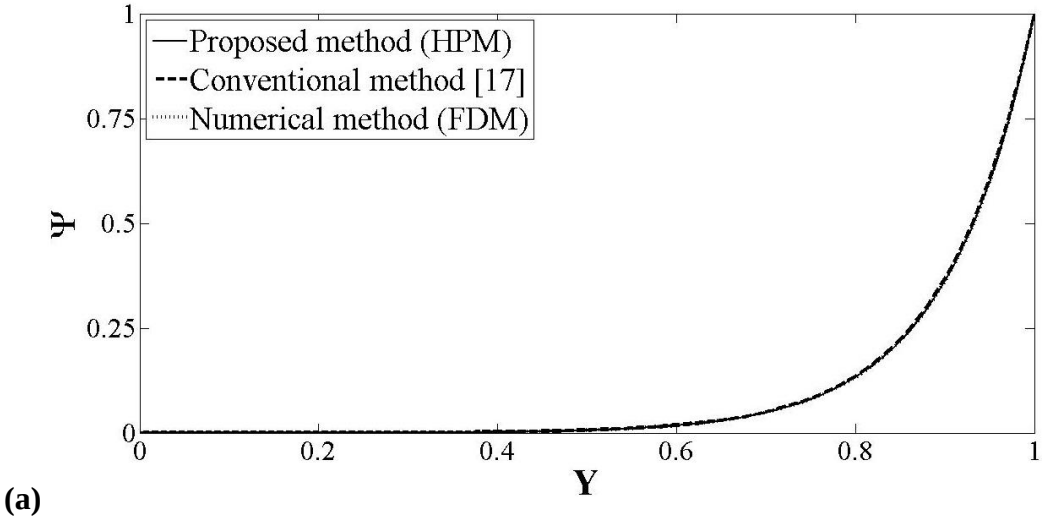

(a)

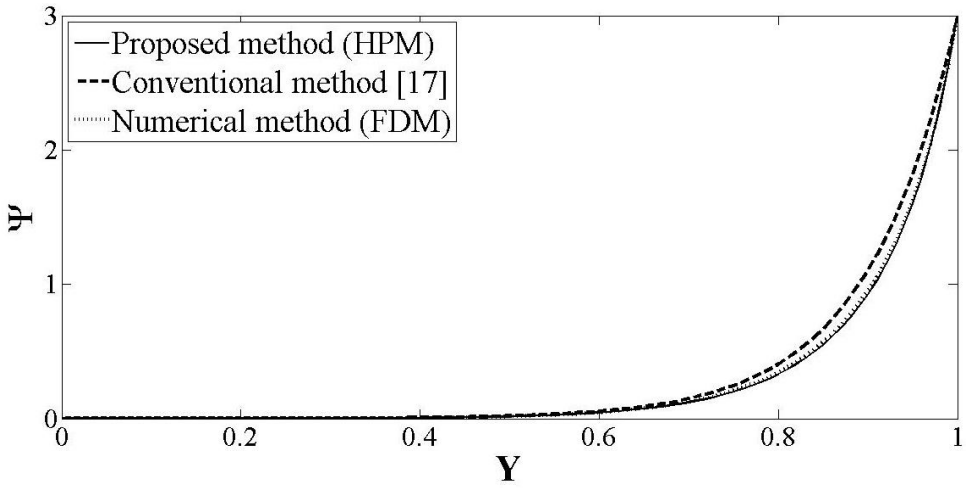

(b)

Fig. 2: Potential distribution for $\lambda = 10$ at (a) $Z = 1$ and (b) $Z = 3$

In the Fig. 2(a, b), the electrical potential obtained by the proposed HPM (without the Debye-Huckel approximation), the conventional method (with the Debye-Huckel approximation) [17] and the FDM are plotted in a comparative way to clearly show the limit of the Debye-Huckel approximation at $Z = 1$ and 3 respectively. The electrokinetic length (λ) is kept constant at 10 to observe the effect of wall zeta potential on the

potential distribution. It is observed that the analytical results obtained by the HPM are in close agreement with the FDM for both the values of Z. As shown in Fig. 2a, the solution based on the conventional method [17] matches well with the numerical solution for smaller value of zeta potential ($Z=1$). But, for higher value of zeta potential ($Z=3$), the conventional method [17] deviates from the numerical results. Therefore, the proposed HPM method without the Debye-Huckel approximation can predict more accurate results for a wide range of wall zeta potential.

Fig. 3(a, b) represent velocity distributions based on the proposed HPM, the conventional method [17] and FDM for $\lambda=10$ at $Z=1$ and 3, respectively. It is clear from both the figures that the proposed HPM method matches well with the numerical method for both the values of wall zeta potential whereas the conventional method [17] deviates for higher value of Z ($Z=3$).

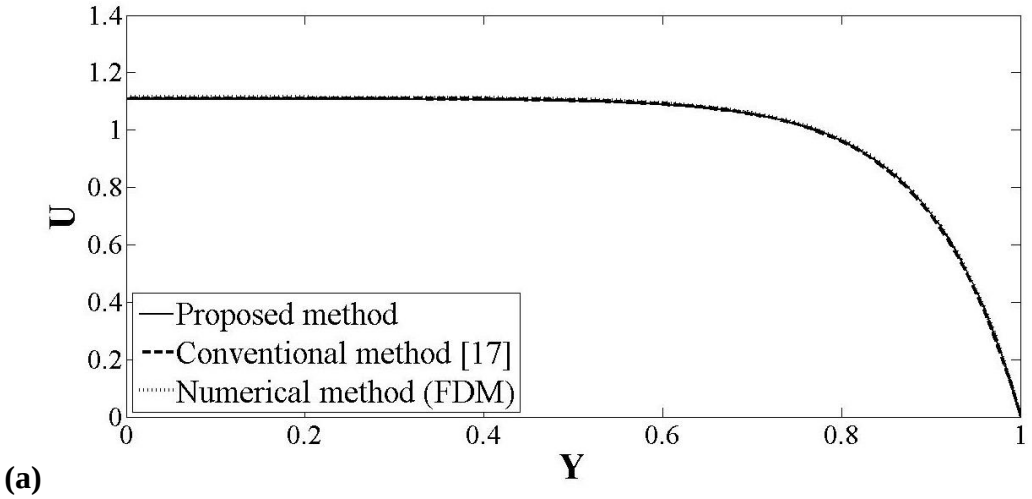

(a)

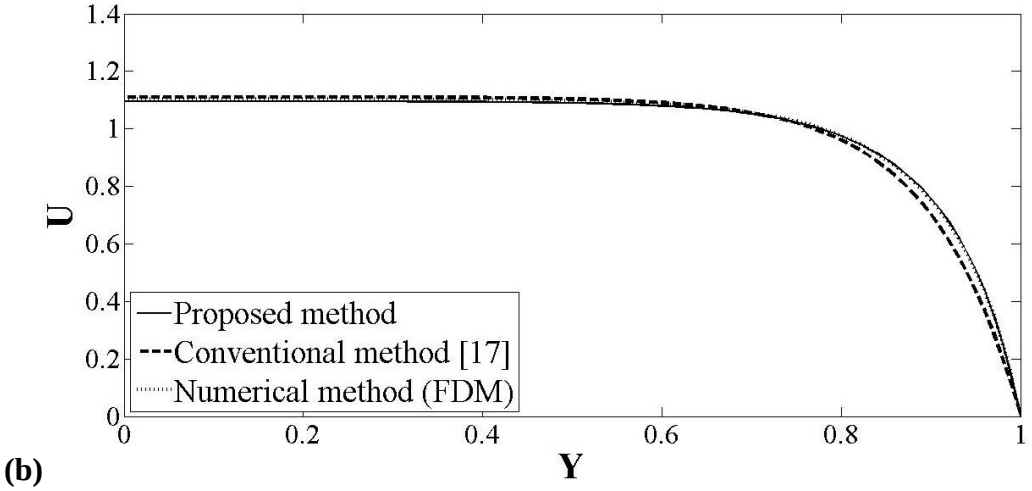

(b)

Fig. 3: Velocity distribution for $\lambda=10$ at (a) $Z=1$ and (b) $Z=3$

The Fig. 4(a, b) represent the temperature distribution for an electrokinetic length of 10 and zeta potential values of 1 and 3. Here the solutions based on the proposed results are compared with the conventional [21] and numerical results. It is observed that the proposed result is in close agreement with the numerical result for both the values of zeta potential whereas, the conventional results [21] show a little deviation from the numerical results close to the plate surface for higher value of zeta potential ($Z = 3$).

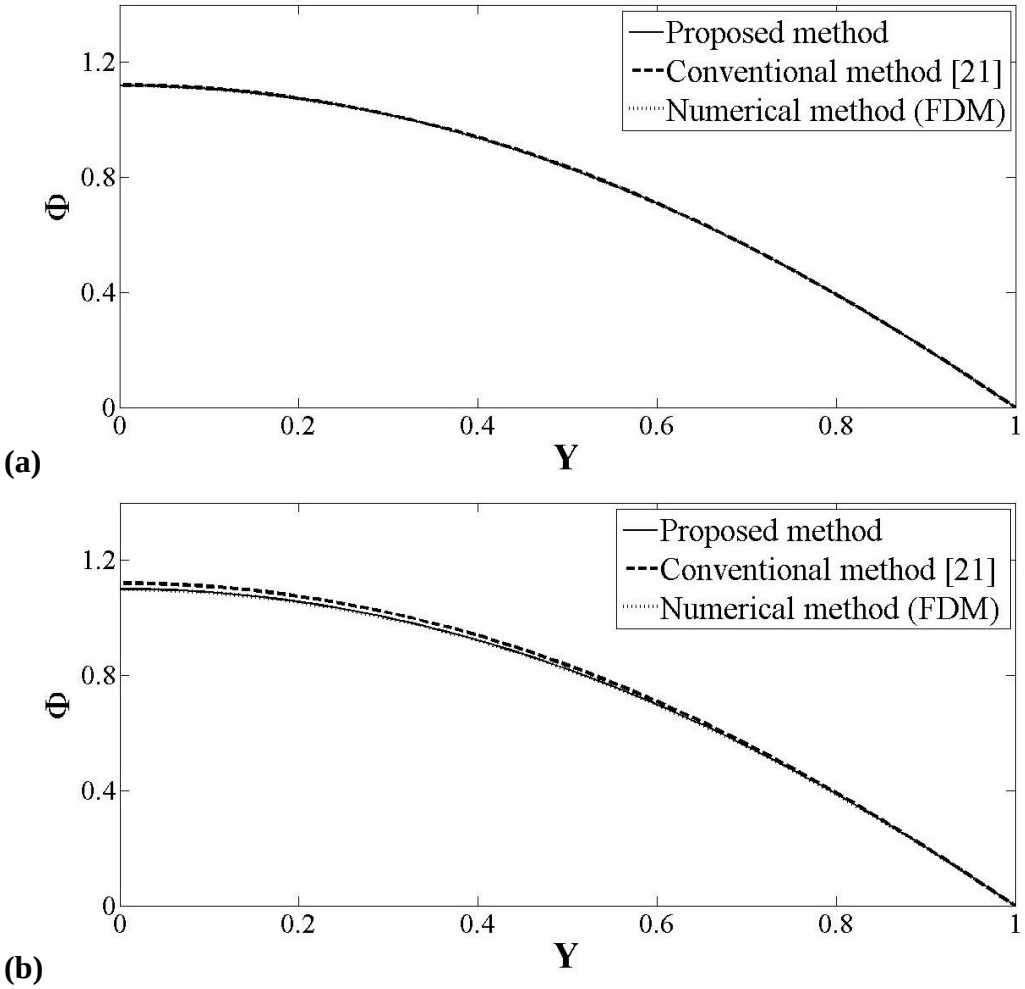

Fig. 4: Temperature distribution for $\lambda = 10$ at (a) $Z = 1$, (b) $Z = 3$

In this section an effort is made to predict the Nusselt number with electrokinetic length for different values of Z ($Z = 1$, 2 and 3) in the Fig. 5. It is observed that for a particular value of Z, Nusselt number decreases steeply with increase in λ. The increase in λ increases the EDL thickness, as a result the resistance to convection heat transfer increases. Thus, Nusselt number decreases as λ increases. It is also noticed that for a particular value of λ, the Nusselt number increases with increase in Z. The increase in the value of Nusselt number with Z can be attributed to the fact that on increasing the

value of Z the presence of EDL can be felt in a region at a greater distance from the wall which lowers the resistance to convection heat transfer, and hence, causes an increase in the value of Nusselt number.

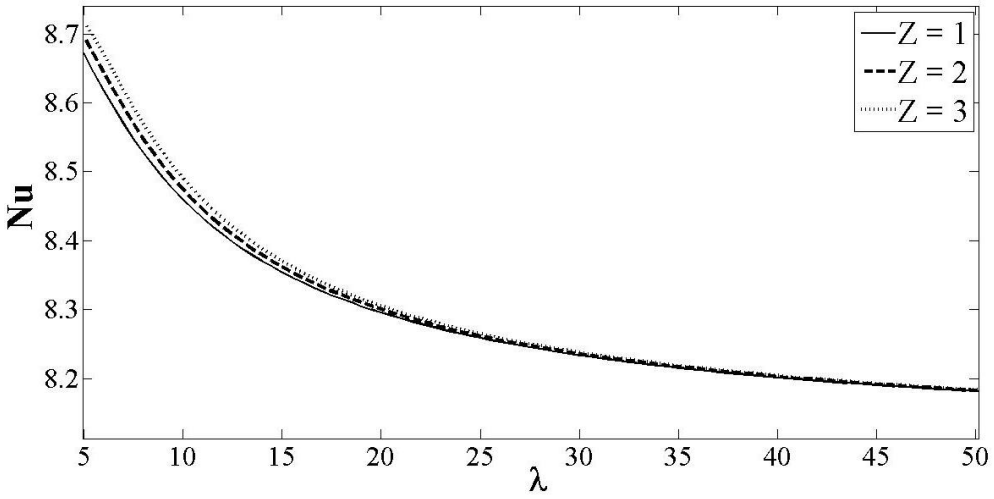

Fig. 5: Variation of Nu with λ for different value of Z

CHAPTER 2

In this section, an analytical study is conducted on a combined pressure driven EOF within a microchannel between two parallel plates. No-slip boundary conditions are considered and the Debye-Huckel linear approximation is ignored. The HPM is considered as an analytical tool to solve the Poisson-Boltzmann equation and determine the electrical potential distribution. While, the reduced forms of the Navier-Stokes and the energy equations are solved analytically for determination of velocity and temperature distributions, respectively.

9. Description of the physical problem

In this section, a microchannel consisting of two parallel plates separated by a distance 2H is considered as shown in Fig. 6. The property variations in the *y*-direction are considered. Half section of the channel (as shown by the hatched area in Fig. 6) is used for analysis. An electric field is induced in the *x*-direction by two plate type electrodes placed apart by length L normal to the parallel plates. A constant pressure gradient is also imposed in the *x*-direction to study the combined effect of both the fields.

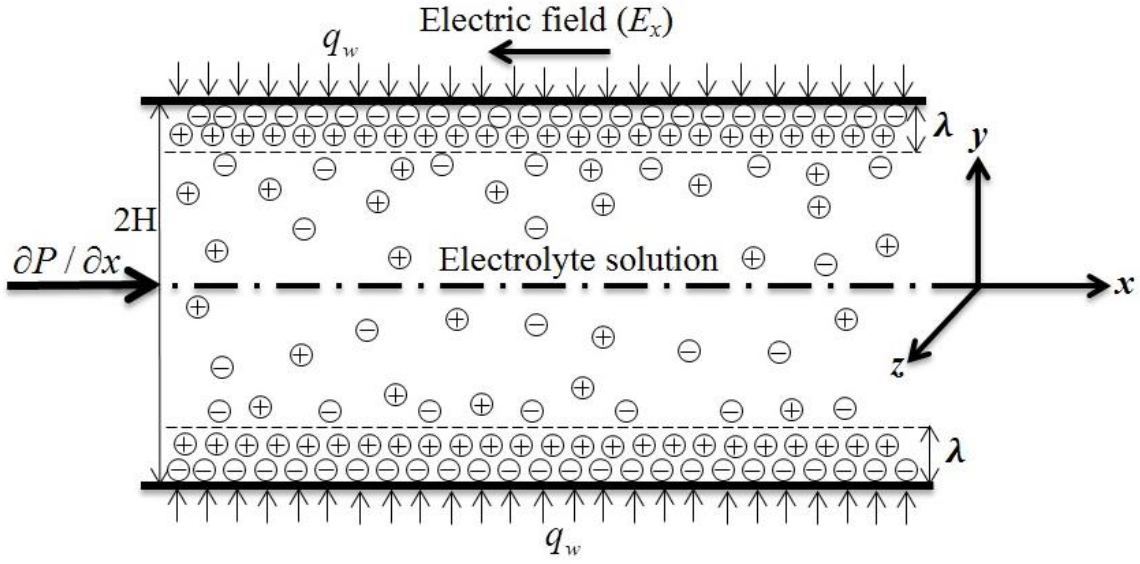

Fig. 6: Schematic of pressure driven EOF through parallel plate microchannel

The following assumptions are made for the mathematical formulation

- The liquid is an incompressible, Newtonian and symmetric electrolyte.
- The thermophysical properties are constant.

- The flow is steady, laminar, hydrodynamically and thermally fully developed.
- No-slip boundary conditions and no wall temperature jump are considered.

10. Mathematical formulation

In the present study, a combined pressure driven electroosmotic flow through a microchannel between two parallel plates is considered. The subsequent governing equations subjected to the respective boundary conditions are considered.

10.1 Poisson-Boltzmann equation

The one dimensional EDL field is described by the Poisson-Boltzmann equation given by the Eq. (1) [15-22] subjected to the following boundary conditions

at $y = 0$, $\partial\psi / \partial y = 0$ and at $y = H$, $\psi = \xi$

10.2 Momentum equation

The Navier-Stokes equation [16, 21, 22] along the *x*-axis is considered by a balance between the shear stresses in the fluid, externally imposed constant pressure gradient and electric field as

$$\mu(\partial^2 u / \partial y^2) - \partial P / \partial x + \rho_f E_x = 0 \tag{32}$$

The above equation is subjected to the following boundary conditions

at $y = 0$, $\partial u / \partial y = 0$ and at $y = H$, $u = 0$

10.3 Energy equation

The steady-state energy equation is given by the Eq. (4) [16, 21, 22]. The corresponding boundary conditions are given as

at $y = 0$, $\partial T / \partial y = 0$ and at $y = H$, $T = T_w$

11. Solution of the governing equations

The governing equations for electrical potential, velocity and temperature distributions have been solved analytically.

11.1 Electric potential distribution

The governing Eq. (1) and its boundary conditions are non-dimensionalized by introducing the dimensionless variables similar to that in Chapter 1 and the Debye-Huckel

approximation is ignored. Here, $\sinh\Psi$ is expanded based on the Taylor series of expansion and Eq. (1) becomes

$$\partial^2\Psi/\partial\mathrm{Y}^2 = \lambda^2(\Psi + \Psi^3/3!+\cdots) \tag{33}$$

The HPM is adopted as an analytical tool to solve the Eq. (33) and the final expression for electrical potential distribution obtained is similar to that in Chapter 1, written as

$$\Psi = \mathrm{A}_1\cosh(\omega\mathrm{Y}) + \mathrm{A}_2\cosh(3\omega\mathrm{Y}) \tag{34}$$

where $\mathrm{A}_1 = \mathrm{Z}/\cosh\omega - \lambda^2\mathrm{Z}^3\cosh 3\omega/[192\omega^2\cosh^4\omega]$ and $\mathrm{A}_2 = \lambda^2\mathrm{Z}^3/[192\omega^2\cosh^3\omega]$

11.2 Velocity distribution

The Navier-Stokes equation becomes

$$\mu(\partial^2 u/\partial y^2) = \partial P/\partial x + \varepsilon E_x\partial^2\psi/\partial y^2 \tag{35}$$

where $\rho_f = -\varepsilon(\partial^2\psi/\partial y^2)$ is the local net charge density.

The Eq. (35) is non-dimensionalized incorporating the following non-dimensional terms

$U = u/u_m$, $\Gamma_1 = -(H^2/\mu u_m)\partial P/\partial x$, $E = E_x L/\xi$ and $\Gamma_2 = 2zen_0\xi H^2/(\mu u_0 L)$

Hence, the non-dimensionalized equation for velocity is written as

$$\partial^2 U/\partial\mathrm{Y}^2 = -\Gamma_1 + (\Gamma_2 E/\lambda^2)(\partial^2\Psi/\partial\mathrm{Y}^2) \tag{36}$$

The corresponding non-dimensional boundary conditions become

at $\mathrm{Y} = 0$, $\partial U/\partial\mathrm{Y} = 0$ and at $\mathrm{Y} = 1$, $U = 0$

Finally, the velocity profile is obtained by integrating Eq. (36) twice with respect to Y with the given boundary conditions as

$$U = \Gamma_1(1-\mathrm{Y}^2)/2 + (\Gamma_2 EZ/\lambda^2)[\{\mathrm{A}_1\cosh(\omega\mathrm{Y}) + \mathrm{A}_2\cosh(3\omega\mathrm{Y})\}/Z - 1] \tag{37}$$

The relation between Γ_1 and Γ_2 is determined from the definition of mean velocity as

$$\int_0^1 U d\mathrm{Y} = 1 \tag{38}$$

and obtained as

$$\Gamma_2 = (\lambda^2/EZ)(1-\Gamma_1/3)/[\{\mathrm{A}_1\sinh(\omega)/(\omega) + \mathrm{A}_2\sinh(3\omega)/(3\omega)\}/Z - 1] \tag{39}$$

Now, the skin friction coefficient, C_f is defined as [8]

$$C_f = 2\tau_w/(\rho U^2) \tag{40}$$

The C_f Re product is obtained as

$$C_f\,\mathrm{Re} = 8\partial U/\partial\mathrm{Y}|_{\mathrm{Y}=1} \tag{41}$$

where $\mathrm{Re} = \rho u_m (4H)/\mu$ is the Reynolds number.

11.3 Temperature distribution

The Eq. (4) for temperature field is reduced by performing scale analysis and the relation obtained is as follows

$$\partial^2\Phi/\partial \mathrm{Y}^2 = (Nu)(U)/4 \tag{42}$$

The corresponding boundary conditions become

at $\mathrm{Y}=0$, $\partial\Phi/\partial\mathrm{Y}=0$ and at $\mathrm{Y}=1$, $\Phi=0$

Substituting the Eq. (37) in Eq. (42) gives

$$\partial^2\Phi/\partial\mathrm{Y}^2 = (Nu/4)[\Gamma_1(1-\mathrm{Y}^2)/2 + (\Gamma_2 EZ/\lambda^2)[\{\mathrm{A}_1\cosh(\omega\mathrm{Y}) + \mathrm{A}_2\cosh(3\omega\mathrm{Y})\}/Z - 1]] \tag{43}$$

Thereafter, the Eq. (43) is integrated twice with respect to Y with the given boundary conditions to yield the temperature distribution as follows

$$\begin{aligned}\Phi = (Nu/4)[\Gamma_1(\mathrm{Y}^2/4 - \mathrm{Y}^4/24 - 5/24) + (\Gamma_2 EZ/\lambda^2)[\{9\mathrm{A}_1\cosh(\omega\mathrm{Y}) + \\ -9\mathrm{A}_1\cosh(\omega) + \mathrm{A}_2\cosh(3\omega\mathrm{Y}) - \mathrm{A}_2\cosh(3\omega)\}/(9Z\omega^2) + (1-\mathrm{Y}^2)/2]]\end{aligned} \tag{44}$$

The mean temperature is defined as

$$\int_0^1 U\Phi d\mathrm{Y} = 1 \tag{45}$$

Finally, the expression of Nusselt number, Nu, is determined at the wall by substituting Eq. (37) and Eq. (44) in the Eq. (45) and solved as

$$\begin{aligned}Nu = 4/\int_0^1 \Gamma_1(1-\mathrm{Y}^2)/2 + (\Gamma_2 EZ/\lambda^2)[\{\mathrm{A}_1\cosh(\omega\mathrm{Y}) + \mathrm{A}_2\cosh(3\omega\mathrm{Y})\}/Z - 1][\Gamma_1(\mathrm{Y}^2/4 + \\ -\mathrm{Y}^4/24 - 5/24) + (\Gamma_2 EZ/\lambda^2)[\{9\mathrm{A}_1\cosh(\omega\mathrm{Y}) - 9\mathrm{A}_1\cosh(\omega) + \mathrm{A}_2\cosh(3\omega\mathrm{Y}) + \\ -\mathrm{A}_2\cosh(3\omega)\}/(9Z\omega^2) + (1-\mathrm{Y}^2)/2]]d\mathrm{Y}\end{aligned} \tag{46}$$

12. Results and discussion

In the segment, a Matlab program is developed to solve the constitutive governing equation. The electrical potential, velocity, temperature fields, skin friction coefficient and Nusselt number are determined. The results obtained are presented in a comparative way with the existing result of Jain and Jansen [21] and numerical method (FDM).

In the Fig. 7(a, b), the potential distributions in the Y direction for an electrokinetic length of 10 are presented at zeta potential values of 1 and 3 respectively. It is observed that the proposed result is in close agreement with the numerical solution for both the zeta potential values of 1 and 3. For smaller value of zeta potential (i.e., Z = 1), the solution based on the Debye-Huckel approximation agrees well with the numerical solution as shown in Fig. 7a whereas deviates more in Fig. 7b for Z = 3. Hence, the proposed method can be used for a large range of zeta potential.

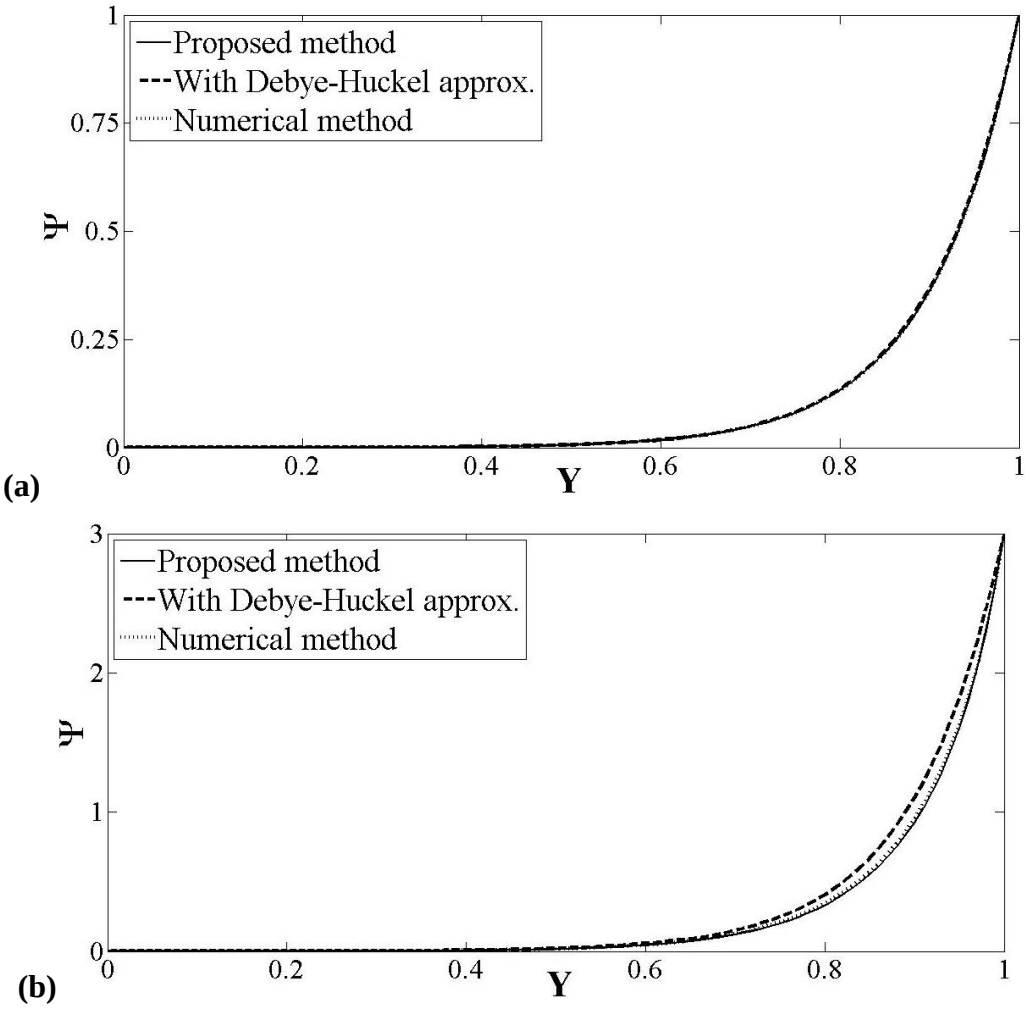

Fig. 7: Potential distribution at (a) Z = 1 and (b) Z = 3 for $\lambda = 10$

The velocity distribution obtained for the combined pressure driven electroosmotic flow are compared with the existing work by Jain and Jansen [21] and numerical results in in Fig. 8(a, b). The proposed results show close agreement with the numerical method for Z = 1 and 3 whereas the existing work shows a little deviation from the numerical method close to the plate surface for Z = 3 as shown in Fig. 8b. This deviation may be due to the effect of the Debye-Huckel approximation considered in the existing work. Hence, the proposed results can predict the velocity distribution for higher values of zeta potential.

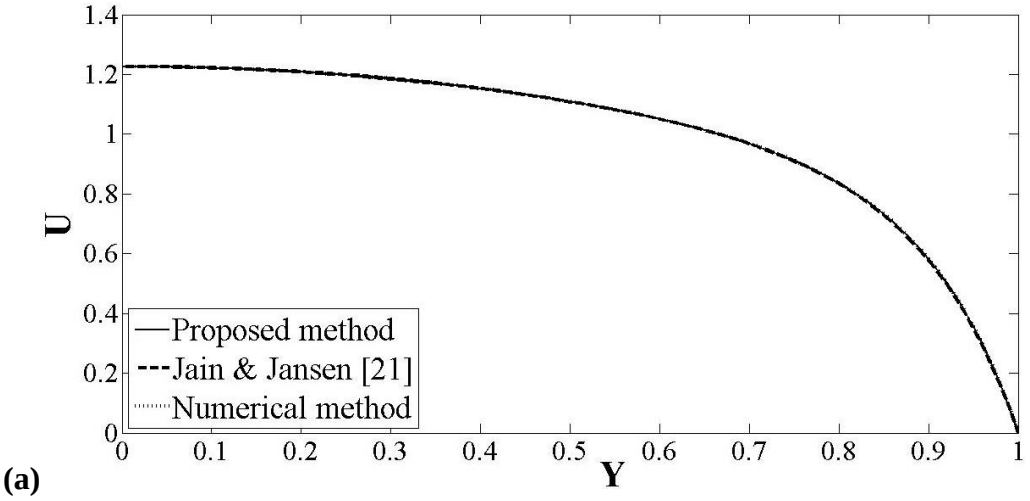

(a)

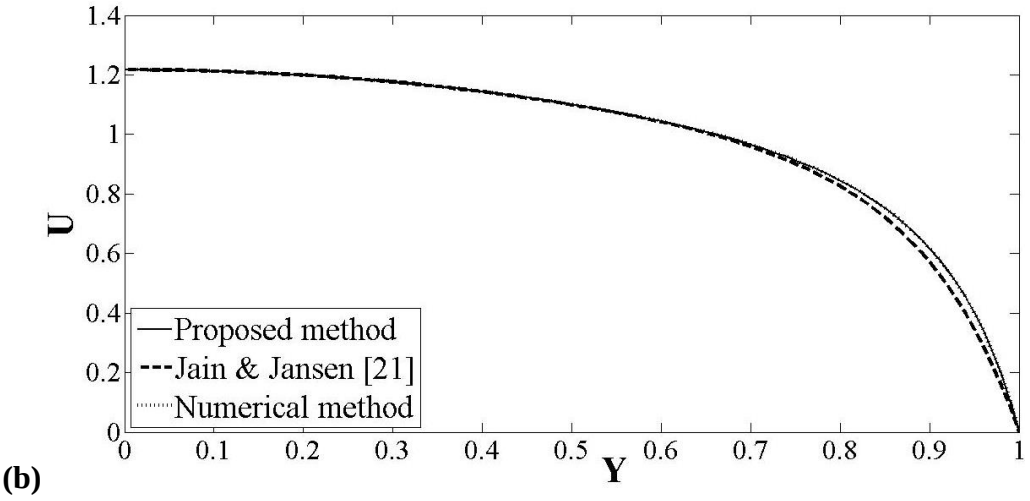

(b)

Fig. 8: Velocity distribution at (a) Z = 1 and (b) Z = 3 for $\lambda = 10$

The Fig. 9(a, b) represent the temperature distribution for an electrokinetic length of 10 and zeta potential values of 1 and 3. Here the solution based on the proposed method is compared with the existing work by Jain and Jansen [21] and numerical results. It is observed that the proposed result is in close agreement with the numerical result for both the zeta potential values of 1 and 3. As a consequence of considering the Debye-Huckel

approximation in the existing work, it shows a little deviation from the numerical result close to the plate surface for Z = 3 as shown in the Fig. 9b. Hence, the proposed method can predict the temperature distribution for higher values of zeta potential.

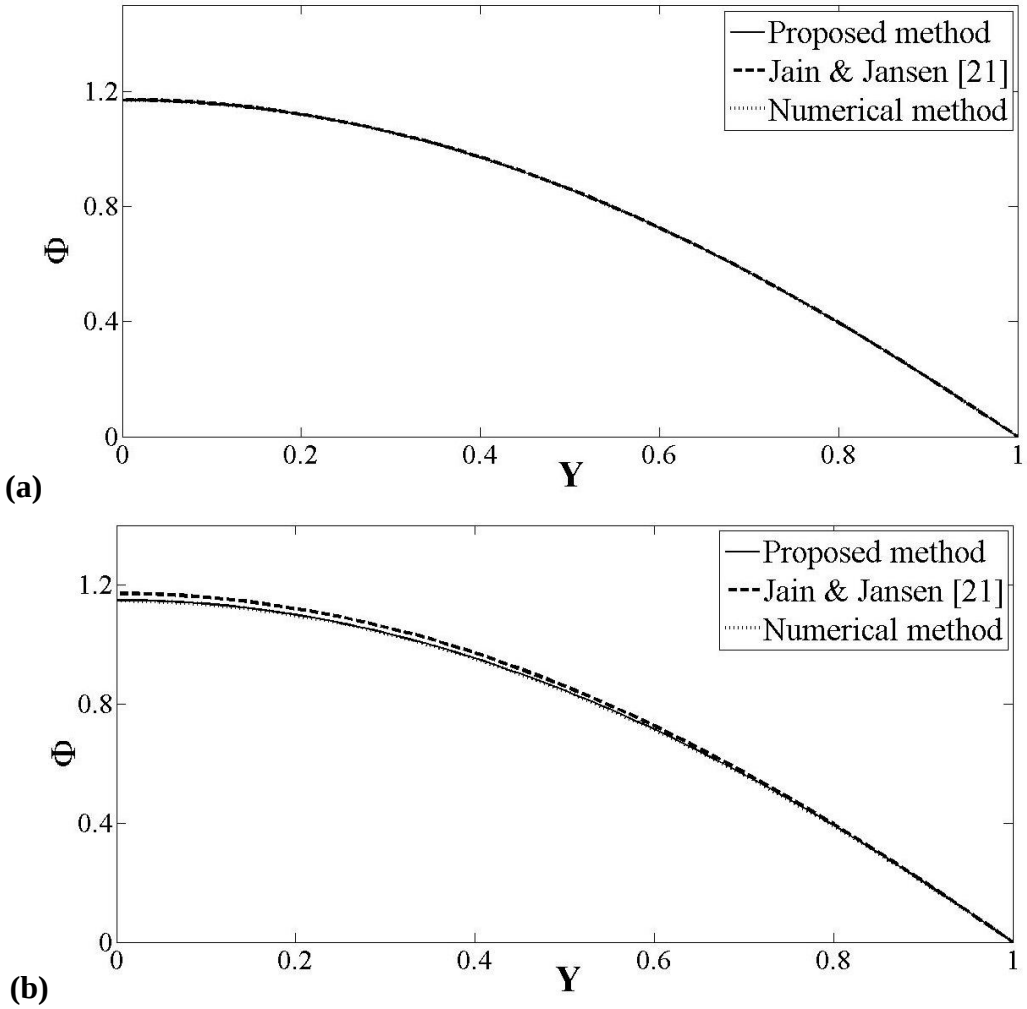

Fig. 9: Temperature distribution at (a) Z = 1 and (b) Z = 3 for $\lambda = 10$

In the Fig. 10(a, b), the product $C_f \,\mathrm{Re}$ and the Nu are presented, respectively, as functions of λ for Z = 1, 2 and 3. It is seen that for a particular value of Z the value of $C_f \,\mathrm{Re}$ decreases with increase in λ. It has also been observed the for a value of λ the $C_f \,\mathrm{Re}$ product increases with rise in Z values. This can be attributed to the fact that on increasing the value of Z the presence of EDL is felt in a region farther away from the wall which enhances the viscosity, and therefore, increases the value of $C_f \,\mathrm{Re}$. The variation of Nu with λ follows the same pattern as that of $C_f \,\mathrm{Re}$.

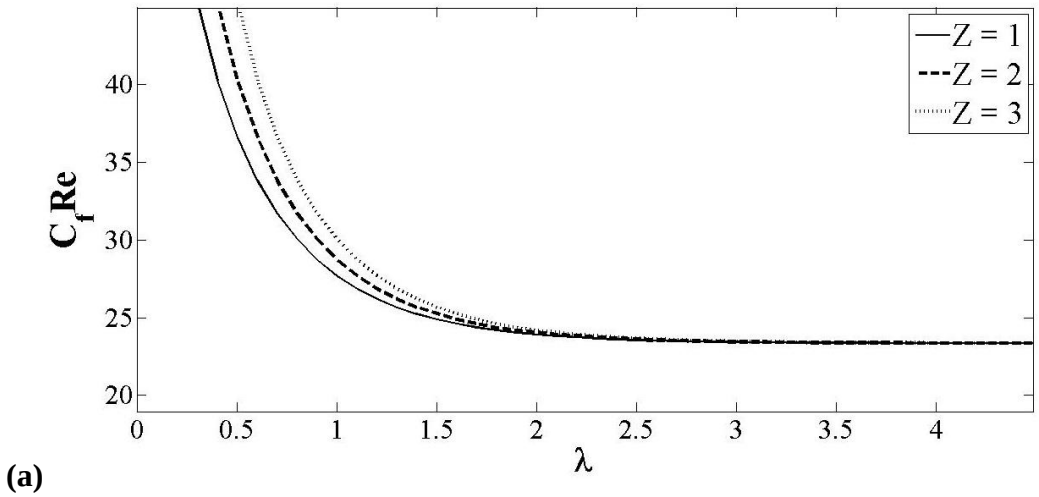

(a)

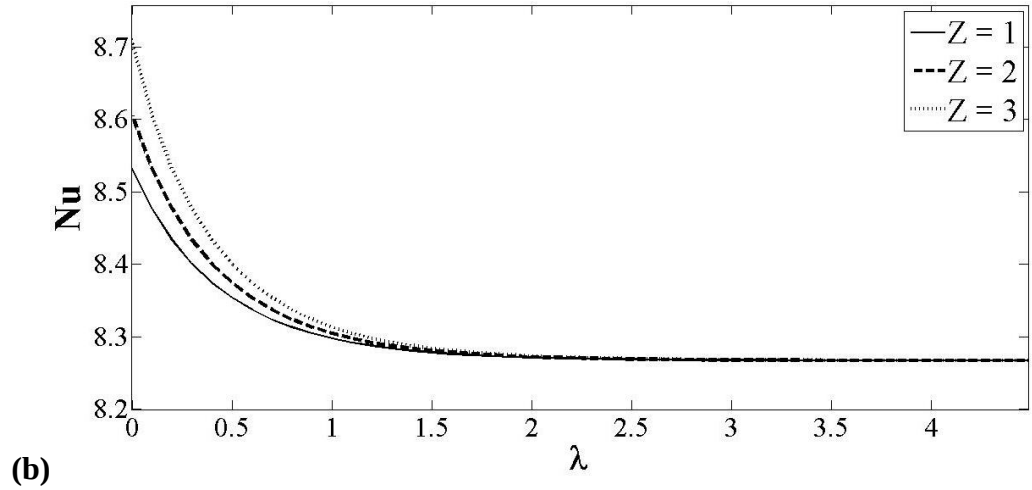

(b)

Fig. 10: Variation of (a) C_f Re product and (b) *Nu* with λ for Z = 1, 2 and 3

CHAPTER 3

In this section, a combined pressure driven electroosmotic flow within a microchannel between two parallel plates with first order slip model is considered. The HPM is adopted as an analytical tool to solve the Poisson-Boltzmann equation. Subsequently, the electric potential distribution is utilized to analytically solve the Navier-Stokes equation and the energy equation for determination of the velocity and temperature distributions, respectively. Finally the skin friction coefficient, Nusselt number and the entropy generation rates are determined from the obtained velocity and temperature distributions.

13. Description of physical problem

In the present work, a microchannel between two parallel plates separated by a distance H is considered as shown in Fig. 11. The plate extends to infinity in *x* and *z* directions. Therefore, property variations are considered in the *y*-direction. Two plate type electrodes are placed apart by length L normal to the parallel plates such that an electric field (E_x) is induced in the *x*-direction. A constant pressure gradient $\partial P/\partial x$ is also imposed in the *x*-direction to study combined effect of both the fields.

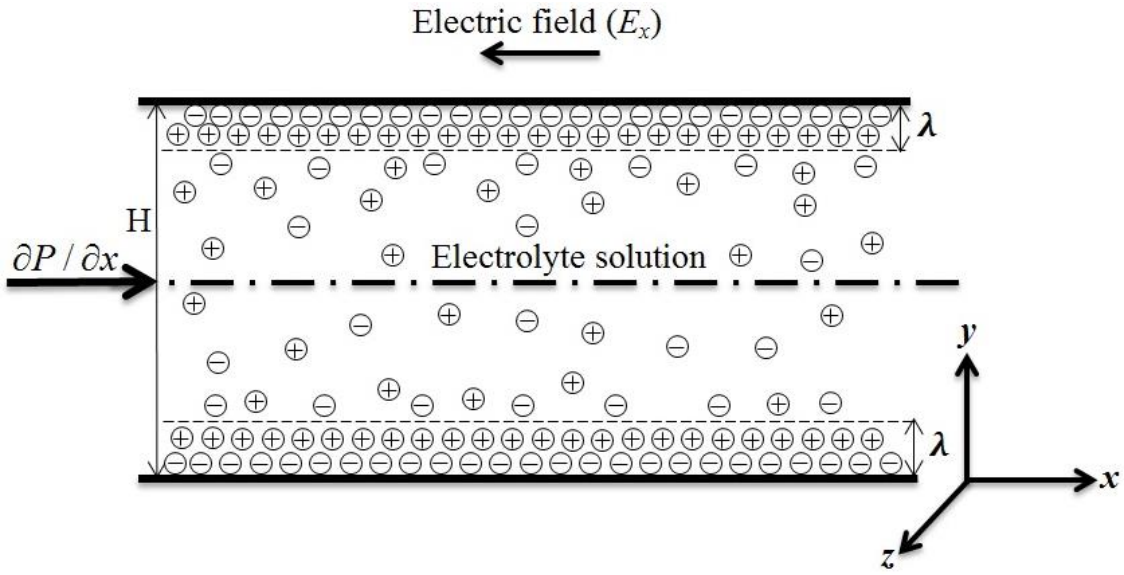

Fig. 11: A combined pressure driven electroosmotic flow between two parallel plates

The following assumptions are made in the present analysis

- The liquid is an incompressible, Newtonian and symmetric electrolyte.

- The thermophysical properties are constant.
- The flow is steady, laminar, hydrodynamically and thermally fully developed.
- First order slip velocity boundary conditions and no temperature jump are considered.

14. Mathematical formulation

In the present study, a combined pressure-driven electroosmotic flow through a microchannel between two parallel plates is considered. The constitutive governing equations subjected to the respective boundary conditions are considered as follows.

14.1 Poisson-Boltzmann equation

The one dimensional EDL field can be described by the Poisson-Boltzmann equation as [15-22]

$$\partial^2\psi/\partial y^2 = (2zen_0/\varepsilon)\sinh(ze\psi/k_bT) \tag{47}$$

The Eq. (46) is subjected to the following boundary conditions

at $y = H/2$, $\partial\psi/\partial y = 0$ and at $y = 0,$ and at $y = H$, $\psi = \xi$

14.2 Momentum equation

The Navier-Stokes equation along the *x*-axis is considered by a balance between the shear stresses in the fluid, externally imposed constant pressure gradient and electric field as [21, 22]

$$\mu(\partial^2u/\partial y^2) - \partial P/\partial x + \rho_f E_x = 0 \tag{48}$$

The above equation is subjected to the following boundary conditions

at $y = 0$, $u = \beta(\partial u/\partial y|_{y=0})$ and at $y = H$, $u = -\beta(\partial u/\partial y|_{y=H})$

14.3 Energy equation

The steady-state energy equation is given as [21, 22]

$$\rho C_p u(\partial T/\partial x) = k(\partial^2 T/\partial y^2) + E_x^2\sigma \tag{49}$$

The boundary conditions are given as

at $y = 0$, $-k(\partial T/\partial y) = q_w$, $T = T_w$ and at $y = H$, $k(\partial T/\partial y) = q_w$, $T = T_w$

15. Solution method

The governing equation for the electrical potential has been solved adopting HPM. Subsequently, the velocity and temperature distributions have been solved analytically based on the obtained electrical potential field.

15.1 Electric potential distribution

The governing Eq. (47) for electrical potential distribution has been solved by adopting HPM but first, it is non-dimensionalized by introducing the dimensionless variables as

$$Y = y/H\ ,\ \Psi = ze\psi/(k_bT),\ Z = 2ze\xi/(k_bT)$$

The non-dimensional form of Eq. (47) becomes

$$\partial^2\Psi/\partial Y^2 = \lambda^2 \sinh\Psi \tag{50}$$

where $\lambda = \kappa H$ and $\kappa = \sqrt{[2z^2e^2n_0/(\varepsilon k_bT)]}$

The corresponding non-dimensional boundary conditions are written as

at $Y = 1/2$, $\partial\Psi/\partial Y = 0$ and at $Y = 0$, and at $Y = 1$, $\Psi = Z$

In the existing work, the Debye-Huckel approximation linearizing $\sinh\Psi$ with Ψ have been used. In the present work, the Debye-Huckel approximation is ignored for Eq. (50) making it nonlinear. Now, $\sinh\Psi$ is expanded based on the Taylor series of expansion as

$$\sinh\Psi = \Psi + \Psi^3/3!+... \tag{51}$$

Substituting the above relation in Eq. (50) results in

$$\partial^2\Psi/\partial Y^2 = \lambda^2(\Psi + \Psi^3/3!+...) \tag{52}$$

The Eq. (52) can be solved by constructing a homotopy as

$$\Psi'' - \omega^2\Psi + p[(\lambda^2 - \omega^2)\Psi + \lambda^2\Psi^2/3] = 0 \tag{53}$$

where, $\Psi'' = \partial^2\Psi/\partial Y^2$, ω is the modified inverse Debye length and $p \in [0,1]$.

The power series in p used to find the solution of Eq. (53) is

$$\Psi = \Psi_0 + p\Psi_1 + p^2\Psi_2 + \cdots \tag{54}$$

Substituting the above expression in Eq. (53) and arranging the coefficients of *p* powers, one can obtain

$$p^0(\Psi_0'' - \omega^2\Psi_0) + p^1[\Psi_1'' - \omega^2\Psi_1 - (\lambda^2 - \omega^2)\Psi_0 - \lambda^2\Psi_0^3/3!] = 0 \tag{55}$$

Equating the coefficients of p^0, p^1 to zero gives

$$p^0: \quad \Psi_0'' - \omega^2 \Psi_0 = 0 \tag{56}$$

$$p^1: \quad \Psi_1'' - \omega^2 \Psi_1 - \left(\lambda^2 - \omega^2\right)\Psi_0 - \lambda^2 \Psi_0^3 / 3! = 0 \tag{57}$$

The Eq. (56) is solved using the boundary conditions

$\Psi_0(0) = Z$, $\Psi_0(1) = Z$ and $\Psi_0'(1/2) = 0$

resulting in

$$\Psi_0 = Z\cosh\{\omega(Y - 1/2)\}/\cosh(\omega/2) \tag{58}$$

Substituting the above expression in Eq. (57) and simplifying the equation gives

$$\begin{aligned}&\Psi_1'' - \omega^2\Psi_1 - (\lambda^2 - \omega^2)Z\cosh\{\omega(Y - 0.5)\}/\cosh(\omega/2) + \\ &- \lambda^2 Z^3[3\cosh\{\omega(\mathrm{Y} - 1/2)\} + \cosh\{3\omega(\mathrm{Y} - 1/2)\}]/[24\cosh^3(\omega/2)] = 0\end{aligned} \tag{59}$$

In order to eliminate $\cos\{\omega(Y - 0.5)\}$ from Eq. (59) the coefficients are collected and equated to zero as

$$(\lambda^2 - \omega^2)Z/\cosh(\omega/2) + \lambda^2 Z^3/[8\cosh^3(\omega/2)] = 0$$

to give the value of ω as follows

$$\omega = \sqrt{[(8\lambda^2 - 8) + \sqrt{(\lambda^2 + 4)^2 + 2z^2}]/2} \tag{60}$$

The Eq. (59) becomes

$$\Psi_1'' - \omega^2\Psi_1 - \lambda^2 Z^3\cosh\{3\omega(\mathrm{Y} - 1/2)\}/[24\cosh^3(\omega/2)] = 0 \tag{61}$$

Now applying the boundary conditions

$\Psi_1(0) = 0$, $\Psi_1(1) = 0$ and $\Psi_1'(1/2) = 0$

the Eq. (61) is solved as

$$\begin{aligned}\Psi_1 = &[\lambda^2 Z^3/192\omega^2\cosh^3(\omega/2)][\cosh\{3\omega(\mathrm{Y} - 1/2)\} + \\ &- \cosh(3\omega/2)\cosh\{\omega(\mathrm{Y} - 1/2)\}/\cosh(\omega/2)]\end{aligned} \tag{62}$$

Substituting the results of Eq. (58) and Eq. (62) in Eq. (54) and considering p = 1, the electric potential distribution is obtained as

$$\Psi = \mathrm{A}_1\cosh\{\omega(\mathrm{Y} - 1/2)\} + \mathrm{A}_2\cosh\{3\omega(\mathrm{Y} - 1/2)\} \tag{63}$$

where $\mathrm{A}_1 = Z/\cosh(\omega/2) - \lambda^2 Z^3\cosh(3\omega/2)/[192\omega^2\cosh^4(\omega/2)]$ and

$\mathrm{A}_2 = \lambda^2 Z^3/[192\omega^2\cosh^3(\omega/2)]$

15.2 Velocity distribution

The Navier-Stokes equation becomes

$$\mu(\partial^2 u/\partial y^2) = \partial P/\partial x + \varepsilon E_x \partial^2\psi/\partial y^2 \tag{64}$$

where $\rho_f = -\varepsilon(\partial^2\psi/\partial y^2)$ is the local net charge density.

The Eq. (64) is non-dimensionalized incorporating the following non-dimensional terms

$U = u/u_m, C_1 = -(H^2/\mu u_m)\partial P/\partial x = \Delta P, C_2 = \varepsilon k_b T E_x/(\mu u_m z e)$ and $\mathrm{B} = u_m\beta/H$

Hence, the equation for the velocity field is written as

$$\partial^2 U/\partial \mathrm{Y}^2 = -C_1 + C_2(\partial^2\Psi/\partial \mathrm{Y}^2) \tag{65}$$

Integrating Eq. (65) twice with respect to Y yields

$$U = -C_1\mathrm{Y}^2/2 + C_2\Psi + a_1\mathrm{Y} + a_2 \tag{66}$$

where a_1 and a_2 are integration constants. The corresponding non-dimensional boundary conditions become

at $\mathrm{Y} = 0, U = \mathrm{B}(\partial U/\partial \mathrm{Y}|_{\mathrm{Y}=0})$ and at $\mathrm{Y} = 1$, $U = -\mathrm{B}(\partial U/\partial \mathrm{Y}|_{\mathrm{Y}=1})$

Applying the above boundary conditions two linear equations are obtained as follows

$$-\mathrm{B}a_1 + a_2 = -C_2\{\Psi(0) + \mathrm{B}\Psi'(0)\} = C_3 \tag{67}$$

$$(1+\mathrm{B})a_1 + a_2 = C_1(\mathrm{B}+1/2) - C_2\{\Psi(1) + \mathrm{B}\Psi'(1)\} = C_4 \tag{68}$$

Solving the Eq. (67) and Eq. (68) the expressions for a_1 and a_2 are determined as

$$a_1 = (C_4 - C_3)/(1+2\mathrm{B}) \tag{69}$$

$$a_2 = \{(1+\mathrm{B})C_3 + \mathrm{B}C_4\}/(1+2\mathrm{B}) \tag{70}$$

Now, the skin friction coefficient C_f is defined as [15]

$$C_f = 2\tau_w/(\rho U^2) \tag{71}$$

The product $C_f\,\mathrm{Re}$ is obtained as

$$C_f\,\mathrm{Re} = 4\partial U/\partial \mathrm{Y}|_{\mathrm{Y}=1} \tag{72}$$

where $\mathrm{Re} = \rho u_m(2H)/\mu$ is the Reynolds number.

15.3 Temperature distribution

The thermally fully developed condition of Eq. (49) for an imposed constant heat flux boundary condition gives

$\partial T/\partial x = \partial T_m/\partial x =$ constant

where $T_m = \int_0^1 UT d\mathrm{Y}$ (73)

The energy balance for a liquid flowing through a microchannel can be expressed as

$$\rho C_p u_m \partial T_m / \partial x = 2q_w / H + E_x^2 \sigma \tag{74}$$

Substituting Eq. (74) in Eq. (49) yields

$$u(2q_w / H + E_x^2 \sigma) / u_m = k(\partial^2 T / \partial y^2) + E_x^2 \sigma \tag{75}$$

The Eq. (75) is non-dimensionalized using the following non-dimensional terms

$\Phi = (T - T_m)/(Hq_w / k)$, $H_1 = 2q_w / H + E_x^2 \sigma$, $q_v = E_x^2 \sigma H / q_w$ and

$\Phi_w = (T_w - T_m)/(Hq_w / k)$

Hence, the non-dimensionalized energy equation becomes

$$\Phi = H_1 U - q_v \tag{76}$$

The non-dimensional boundary conditions are

at $\mathrm{Y} = 0$, $\partial\Phi / \partial \mathrm{Y} = -1$, $\Phi = \Phi_w$ and at $\mathrm{Y} = 1$, $\partial\Phi / \partial \mathrm{Y} = 1$, $\Phi = \Phi_w$

Integrating Eq. (76) twice with respect to Y subjected to the above boundary conditions yields

$$\begin{aligned}\Phi_w - \Phi = {} & H_1 C_1 (\mathrm{Y}^4 - \mathrm{Y})/24 + H_1 C_2 [\mathrm{A}_1 \{\cosh(\omega/2) - \cosh\omega(\mathrm{Y} - 1/2)\}/\omega^2 + \\ & + \mathrm{A}_2 \{\cosh(3\omega/2)\}/9\omega^2 - \cosh 3\omega(\mathrm{Y} - 1/2)] + H_1 a_1 (\mathrm{Y} - \mathrm{Y}^3)/6 + \\ & + H_1 a_2 (\mathrm{Y} - \mathrm{Y}^2)/2 + H_1 q_v (\mathrm{Y}^2 - \mathrm{Y})/2\end{aligned} \tag{77}$$

The fully developed Nusselt number at the top and bottom plates is expressed as [22]

$$Nu = q_w H / \{k(T_w - T_m)\} = 1/(\Phi_w - \Phi_m) \tag{78}$$

where

$$\Phi_w - \Phi_m = \int_0^1 U(\Phi_w - \Phi) d\mathrm{Y} \tag{79}$$

15.4 Entropy generation rate

In this section an effort is made to determine entropy generation rate. The local volumetric entropy generation rate is described as [24-26]

$$S_G = S_{GH} + S_{GJ} + S_{GV} \tag{80}$$

where S_{GH}, S_{GJ} and S_{GV} are the local volumetric entropy generation rates due to heat diffusion, Joule heating and viscous dissipation, respectively, as described below

$$S_{GH} = k(\partial T / \partial y)^2 / T^2 \tag{81}$$

$$S_{GJ} = \sigma E_x^2 / T \tag{82}$$

$$S_{GV} = \mu(\partial U / \partial y)^2 / T \tag{83}$$

S_G is non-dimensionalized by introducing the following non-dimensional terms

$$S_H = (\partial \Phi / \partial \mathrm{Y})^2 / (\Phi + \theta)^2 \tag{84}$$

$$S_J = q_v / (\Phi + \theta) \tag{85}$$

$$S_V = Br(\partial U / \partial \mathrm{Y})^2 / (\Phi + \theta) \tag{86}$$

where

$\theta = kT_w / (Hq_w)$ and $\mathrm{B}r = \mu u_m^2 / (Hq_w)$ is the Brinkmann number.

The non-dimensional global entropy generation rate is expressed as [24-26]

$$S_{total} = \int_0^{1/2} (S_H + S_J + S_V) d\mathrm{Y} \tag{87}$$

16. Result and discussion

In the present study, a combined pressure driven electroosmotic flow between two parallel plates with first order slip boundary conditions is considered. The electrical potential, velocity, temperature fields, skin friction coefficient, Nusselt number and the entropy generation rates are determined. Finally, a Matlab program is developed to solve the constitutive governing equations. Different parametric studies are conducted on the results obtained.

16.1 Effect of wall zeta potential on the potential distribution

In the Fig. 12, the non-dimensional potential distribution (Ψ) in the direction normal to the parallel plates (Y- direction) is presented for $Z = 1, 2$ and 4 considering an electrokinetic length (λ) of 10. It is observed that Ψ value increases from the centre of the microchannel and attains maximum value at the walls. Moreover, the value of Ψ increases with increase in Z.

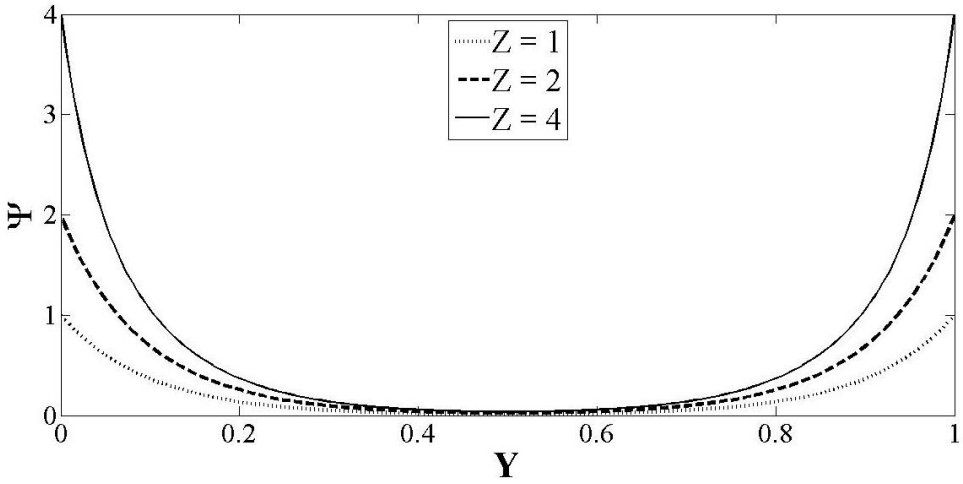

Fig. 12: Potential distribution for different values of zeta potential ($\lambda = 10$)

16.2 Effect of slip coefficient and pressure gradient on the velocity distribution

In Fig. 13, the non-dimensional velocity distribution (U) is presented with Y at $B = 0$, 0.05 and 0.1 for $\lambda = 10, Z = 1$ and $\Delta P = 1.9$. The velocity profile for $B = 0$ corresponds to the familiar velocity profile with no slip boundary condition whereas the

velocity profiles for $B = 0.05$ and 0.1 clearly depict that the increase in B leads to higher values of U.

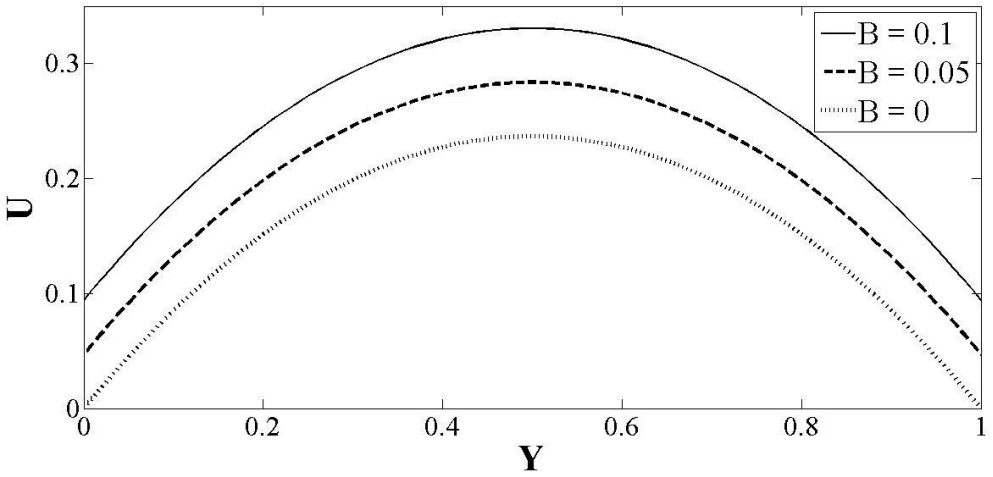

Fig. 13: Velocity distribution for different values of slip coefficient ($\lambda = 10, Z = 1, \Delta P = 1.9$)

The Fig. 14 shows the variation of with U for $\Delta P = 0.9, 1.9$ and 2.8 considering $B = 0.05$. It is observed that U increases with increase in ΔP. The rate of increase of U is more as the ΔP value increases.

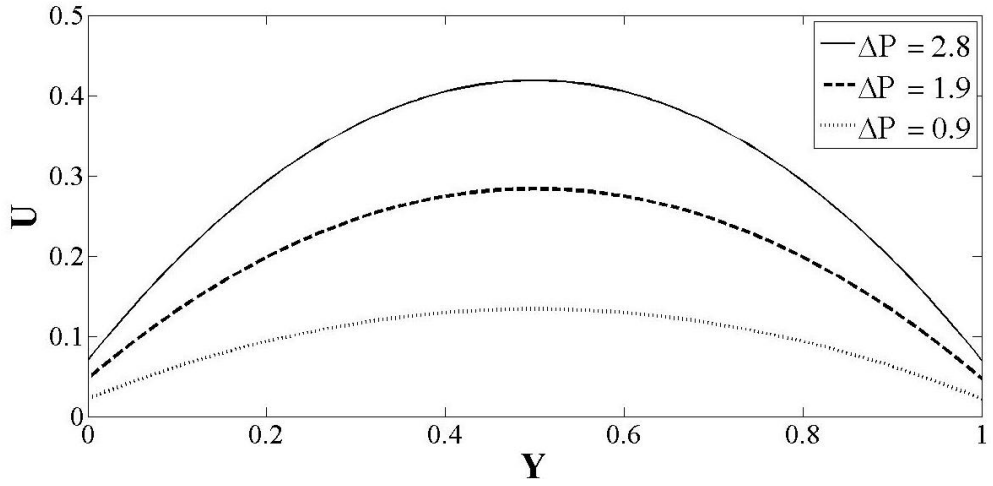

Fig. 14: Velocity distribution for different values of pressure gradient ($\lambda = 10$, $Z = 1, B = 0.05$)

16.3 Effect of wall zeta potential on the C_f Re product

In the Fig. 15, the C_f Re product is presented as a function of λ for $Z = 1$, 2 and 3. It is seen that for a particular value of Z, the value of C_f Re decreases with increase in λ. With increase in λ, EDL field increases resulting an increase of C_f. At the same time

viscosity increases resulting an decrease in Re. But, the rate of decrease of Re is much faster than the rate of increase of C_f. As a result, $C_f \mathrm{Re}$ product decreases with increase in λ. It has also been observed that for a particular value of λ, the $C_f \mathrm{Re}$ product increases with rise in Z. This can be attributed to the fact that on increasing the value of Z, the presence of EDL is felt in a region farther away from the wall which enhances the viscosity, and therefore, increases the value of $C_f \mathrm{Re}$.

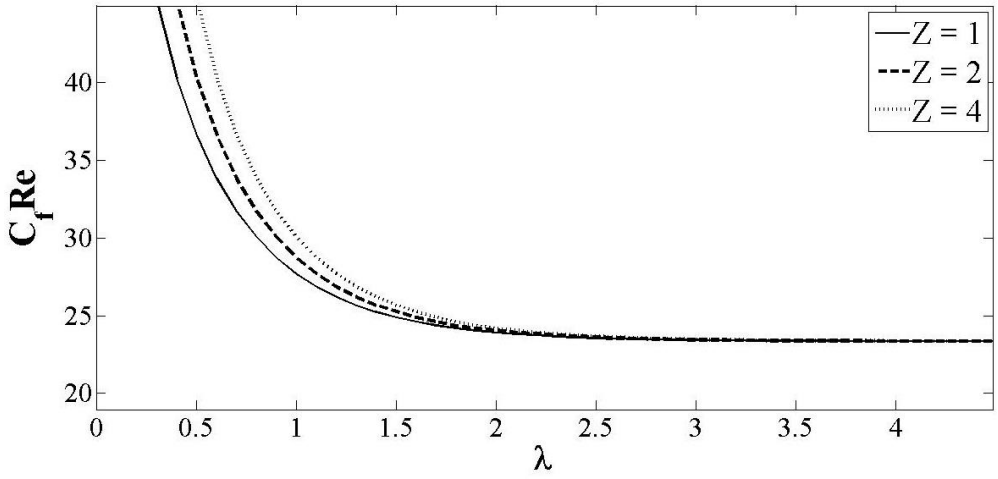

Fig. 15: Variation of C_f Re product with λ for $Z = 1, 2$ and 3

16.4 Effect of slip coefficient and pressure gradient on the temperature distribution

The Fig. 16 represents the non-dimensional temperature distribution at various values of B $(0, 0.05, 0.1)$ for $\lambda = 10, Z = 1$ and $\Delta P = 1.9$. It is observed that the difference between wall and local temperatures attains a maximum value at the centre of the microchannel. With increase in B the velocity field tends to increase and thus, the convection heat transfer increases. As a result, the maximum value of temperature distribution decreases with increase in B.

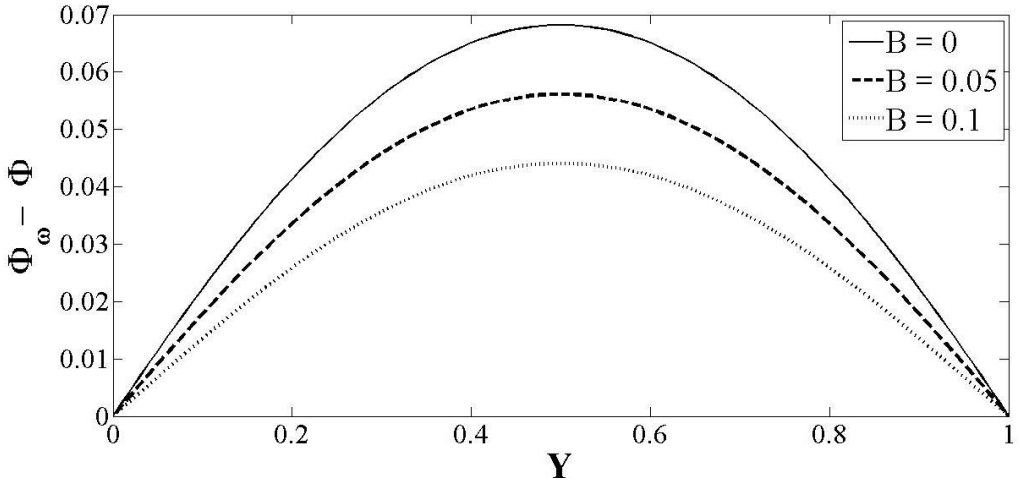

Fig. 16: Temperature distribution for different values of slip coefficient ($\lambda = 10$, $Z = 1, \Delta P = 1.9$)

In Fig. 17, ΔP value is varied $(0.9, 1.9, 2.8)$ to study its effect on the temperature distribution considering $B = 0.05$. It is evident that the maximum temperature decrease with increase in ΔP.

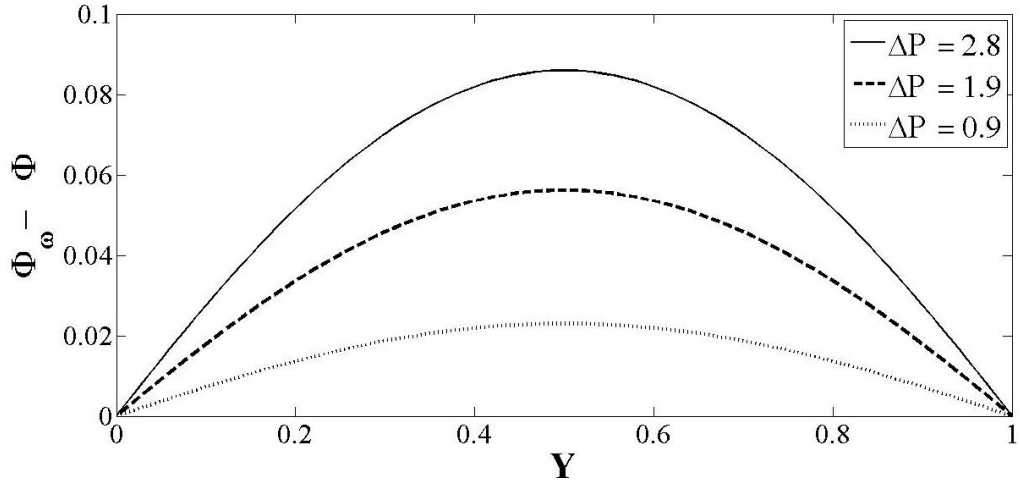

Fig. 17: Temperature distribution for different values of pressure gradient ($\lambda = 10$, $Z = 1, B = 0.05$)

16.5 Effect of wall zeta potential and electrokinetic length on Nusselt number

In this section, the effect of various flow parameters on Nu is studied. Fig. 18 shows the variation of Nu with λ for $Z = 1, 2$ and 4 considering $\Delta P = 1.9, B = 0.05$. It is seen that Nu first increases, attains a peak value and then decreases. This may be explained as the creation of small turbulences in the flow field due to ionic distribution for smaller

value of λ. Whereas for a larger value of λ, the wall is completely surrounded by counter-ions which in turns reduces the disturbances in the flow causing Nu to decrease with λ. It is also noticed from the same figure that for a particular value of λ, Nu increases with increase in Z. The effect of the electrostatic potential near the wall dominates with increase in Z resulting in increase in the apparent viscosity which causes Nu to increase.

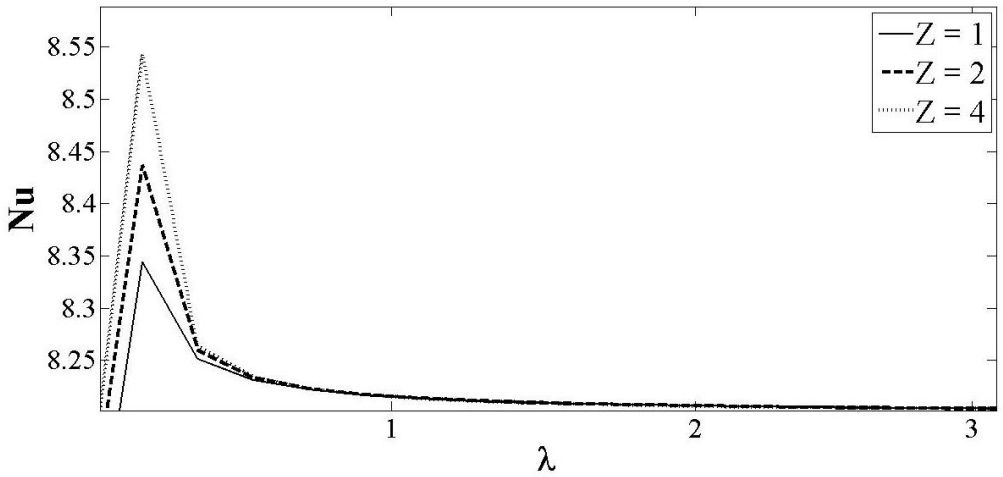

Fig. 18: Variation of Nu with λ for different values of Z ($\Delta P = 1.9, \mathrm{B} = 0.05$)

In the Fig. 19, Nu is presented with B for $\lambda = 10, 20, 40$ where $Z = 1$ and $\Delta P = 1.9$. It is observed that Nu increases with increase in B. An increase in B increases U which in turn enhances the heat transfer coefficient resulting an increase in Nu.

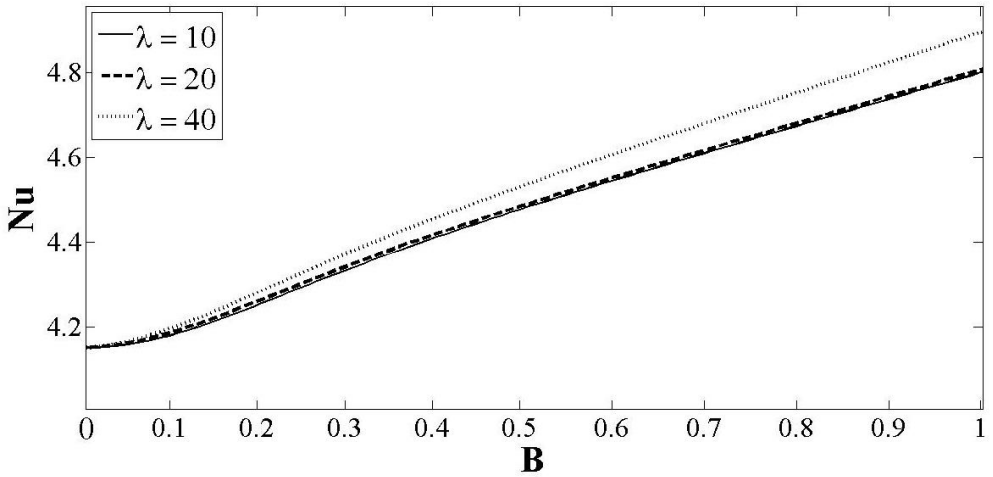

Fig. 19: Variation of Nu with B for different values of λ ($Z = 1, \Delta P = 1.9$)

16.6 Effect of pressure gradient on the entropy generation

This section deals with the effect of ΔP and Br on the entropy generation rates. The Fig. 20 shows the variation of S_G with Y for $\Delta P = 0.9, 1.9$ and 2.8 considering $\lambda = 10$, $Z = 1, \mathrm{B} = 0.05, \mathrm{Br} = 0.02$ and $\theta = 1000$. It is observed that S_G rises from the centre of the microchannel and attains a maximum value at the wall. It is also noticed that S_G value increases with increase in ΔP upto a certain value of Y ($\mathrm{Y} = 0.42$). This is due to the effect of electrical potential which is predominant near the wall and diminishes near the centre. A part of the work associated with fluid delivery and heat transfer is lost in the process of electroosmotic flow, whose value is proportional to that of S_G. The lost work increases with increase in ΔP resulting an increase in S_G.

In the Fig. 21, S_{total} is presented with Br for $\Delta P = 0.9,\ 1.9$ and 2.8. It is observed that S_{total} increases with both increase in ΔP and Br. The effect of viscous dissipation increases with increase in Br, resulting an increased value of S_{total}. Moreover, with rise in $\Delta P, U$ increases causing S_{total} to increase.

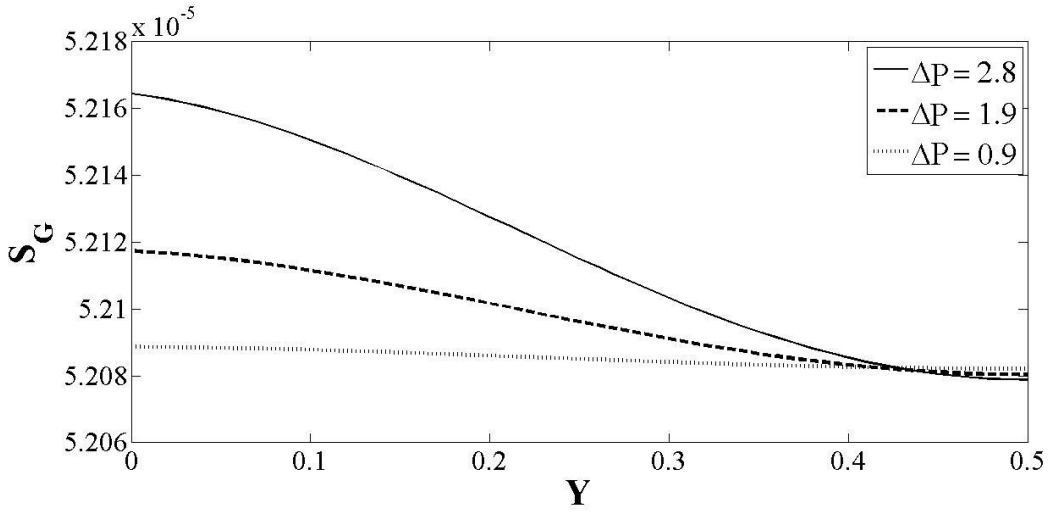

Fig. 20: Variation of S_G with Y for different values of pressure gradient ($\lambda = 10$, $Z = 1$, $\mathrm{B} = 0.05, \mathrm{Br} = 0.02$ and $\theta = 1000$)

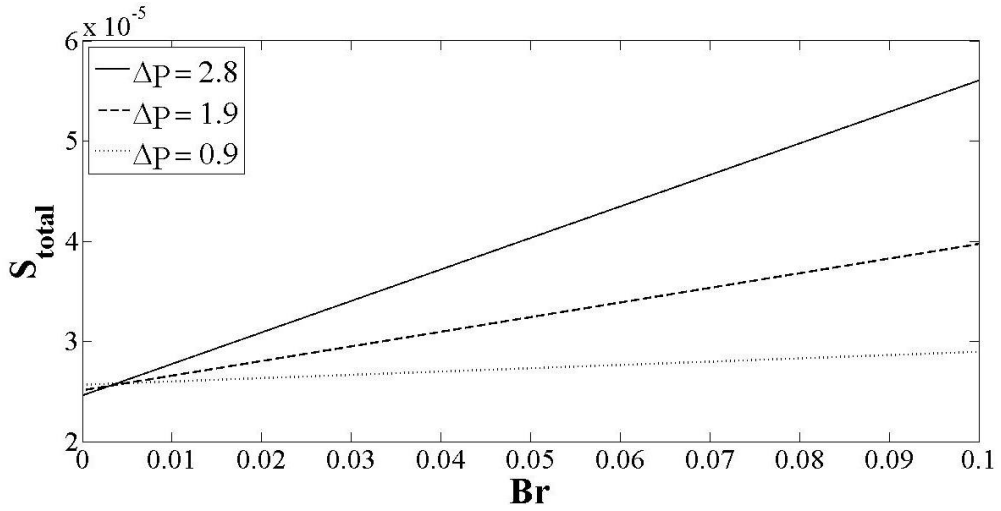

Fig. 21: Variation of S_{total} with Br for different values of pressure gradient ($\lambda = 10$, $Z = 1$, $B = 0.05$ and $\theta = 1000$)

16.7 Validation of the present work

The present analytical model for the pressure driven electroosmotic flow through a microchannel between two parallel plates is validated with the existing work by Ngoma and Erchiqui [22]. The Fig. 22 represents the temperature distribution based on present work with the Ngoma and Erchiqui [22] as a function of Y for $\lambda = 10, Z = 1, \Delta P = 1.9$ and $B = 0.05$. It is observed that the proposed result agrees well with the Ngoma and Erchiqui [22]. Therefore, the present analysis can be extended for analysis of pressure driven electroosmotic flow between two parallel plates.

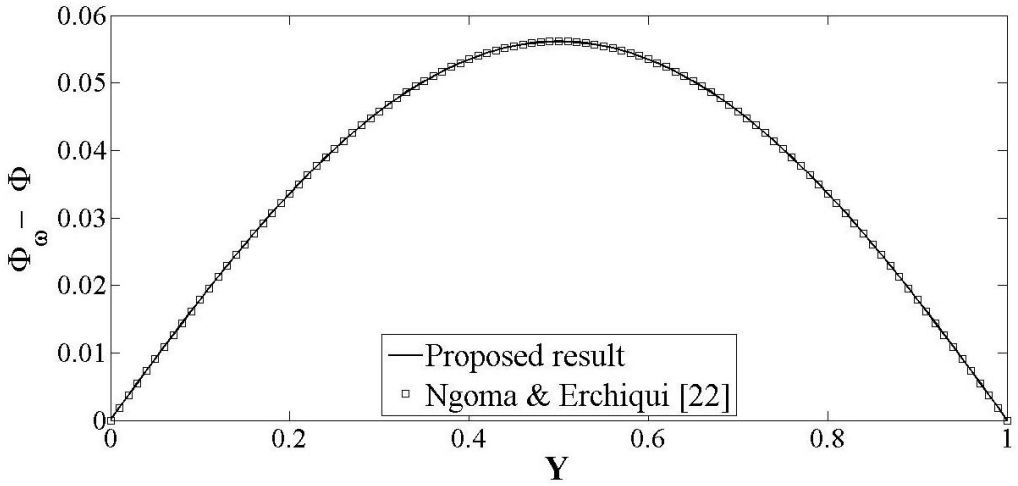

Fig. 22: Temperature distribution with Y ($\lambda = 10, Z = 1, \Delta P = 1.9$ and $B = 0.05$)

17. Conclusion

The present work proposes analytical solutions based on HPM to study the characteristics of a simple EOF and a combined pressure driven EOF within a parallel plate microchannel with both no-slip and first order slip boundary conditions. The electrical potential, velocity and temperature distributions are obtained by solving the Poisson-Boltzmann equation without Debye-Huckel approximation, the Navier–Stokes equation and energy equation, respectively. The HPM is used to solve the nonlinear Poisson-Boltzmann equation to determine the electrical potential distribution. The potential distribution obtained is subsequently used to solve the Navier Stokes and the energy equations to determine analytically the velocity and temperature distributions, respectively. C_f and Nu are determined based on the velocity and temperature profiles respectively. Finally, entropy generation rates are determined.

The observations in Chapter 1 are as follows

- The non-dimensional potential distribution (Ψ), velocity distribution (U) and temperature distribution (Φ) are presented with the non-dimensional distance between the plates (Y) for $\lambda = 10$ and different values of Z. The results of the proposed method match well with that of the numerical method (FDM) while, the conventional method shows deviation at higher value of Z.
- The variation of Nu with λ is presented for $Z = 1,\ 2$ and 3. Nu is found to decrease with λ whereas, its value for a particular value of λ increases with increase in Z.

Chapter 2 shows the following observations

- Ψ, U and Φ are presented with Y for $\lambda = 10$ and $Z = 1$ and 3. The results of the proposed method show good agreement with that of the numerical method (FDM) for both the values of Z, while the conventional method shows deviation at $Z = 3$.
- Nu and $C_f \mathrm{Re}$ product are varied with λ for different values of Z. Both Nu and $C_f \mathrm{Re}$ product are found to decrease with increase in λ but increase with increase of Z for a particular value of λ.

Chapter 3 presents the following observations

- Ψ is presented with Y for $\lambda = 10$ and different values of Z. Ψ is found to attain its maximum value at the wall which increase with increase of Z.
- The effect of B and ΔP on U and $\Phi_w - \Phi$ is studied considering $\lambda = 10$ and $Z = 1$. It is seen that U increases with increase in both B and ΔP, whereas $\Phi_w - \Phi$ decreases in both the cases.
- The variation of $C_f \mathrm{Re}$ product with λ is analyzed for different values of Z (1, 2, 4). It is observed that $C_f \mathrm{Re}$ product decreases with increase in λ, while increases with increase in Z.
- The variations of Nu with λ and B are presented for different values of Z and λ, respectively. Nu first increase, attains a peak value and decreases with λ, while the peak value increases with Z. It is also observed that Nu increases with increase in B.
- S_G is presented with Y considering $\lambda = 10, Z = 1, B = 0.05, Br = 0.02$ and $\theta = 1000$, while S_{total} is presented as a function of Br varying the values of ΔP ($0.9, 1.9, 2.8$). It is evident that both S_G and S_{total} increase with increase in ΔP.
- Finally, the temperature distribution for $\lambda = 10, Z = 1, \Delta P = 1.9, B = 0.05$ determined by the proposed method is compared with that obtained by Ngoma and Erchiqui [22] and it is seen that they show perfect harmony.

18. Future work

In the present work, analytical solutions have been proposed for simple EOF and combined pressure driven EOF within microchannel between two parallel plates with both no-slip and first order slip boundary conditions. The velocity profile may be determined considering second order slip boundary conditions. The energy equation has been solved ignoring any temperature jump. Therefore, first or second order temperature jump may be taken into account for future work. Moreover, the present work may be carried out for rectangular microchannel rather than parallel plate microchannel.

19. Reference

[1] Coffel J., Nuxoll E., BioMEMS for biosensors and closed-loop drug delivery, International Journal of Pharmaceutics 544 (2) (2018) 335-349

[2] Lin B., Levchenko A., Microfluidic technologies for studying synthetic circuits, Current Opinion in Chemical Biology, 16 (3-4) (2012) 307-317

[3] Cooney C. G., Towe B. C., A thermopneumatic dispensing micropump, Sensors and Actuators 116 (2004) 519-524

[4] Kabir M. et al., Piezoelectric MEMS acoustic emission sensors, Sensors and Actuators 279 (2018) 53-64

[5] Ni H., Amme R. C., Ion redistribution in an electric double layer, Journal of Colloid and Interface Science 260 (2003) 344-348.

[6] Manciu M. et al., On the surface tension and Zeta potential of electrolyte solutions, Advances in Colloid and Interface Science 244(2016) 90-99

[7] Xie Z. Y. et al., Thermal transport of magnetohydrodynamic electroosmotic flow in circular cylindrical microchannels, International Journal of Heat and Mass Transfer 119 (2018) 355-364

[8] Wang C. et al., Characterization of electroosmotic flow in rectangular microchannels, International Journal of Heat and Mass Transfer 50 (2007) 3115-3121

[9] Tokiwa F., Electrostatic and electrokinetic potentials of surfactant micelles in aqueous solutions, Advances in Colloid and Interface Science 3 (4) (1972) 389-424

[10] Bohinc K. et al., Incorporation of ion and solvent structure into mean-field modeling of the electric double layer, Advances in Colloid and Interface Science 249 (2017) 220-233

[11] Drab M., Kralj-Iglic V., Diffuse electric double layer in planar nanostructures due to Fermi-Dirac statistics, Electrochimica Acta 204 (2016) 154-159

[12] Burgreen D., Nakache F.R., Electrokinetic flow in ultrafine capillary silts, The Journal of Physical Chemistry 68 (5) (1964) 1084-1091

[13] Jooybari H. S., Chen Z., Analytical solutions of the Poisson-Boltzmann equation within an interstitial electrical double layer in various geometries, Chemical Physics 522 (2019) 147-162

[14] Khan M. et al., Exact solution of an electroosmotic flow for generalized Burgers fluid in cylindrical domain, Results in Physics 6 (2016) 933-939

[15] Steffen V. et al., Debye-Huckel approximation for simplification of ions adsorption equilibrium model based on Poisson–Boltzmann equation, Surfaces and Interfaces 10 (2018) 144-148

[16] Yang C., Li D.Q., Electrokinetic effects on pressure-driven liquid flows in rectangular microchannels, J. Colloid Interf. Sci. 194 (1) (1997) 95-107

[17] Kandlikar S. et al., (2006) Heat Transfer and Fluid Flow in Minichannels and Microchannels. 1st edn. Great Britain: Elsevier Ltd, 137-142

[18] Min JY et al., A novel approach to analysis of electroosmotic pumping through rectangular-shaped microchannels, Sensors and Actuators B 120 (2006) 305-312,

[19] Tunc G., Bayazitoglu Y., Heat transfer in rectangular microchannel, International Journal of Heat and Mass Transfer 45 (2002) 765-773

[20] Mala G. M. et al., Heat transfer and fluid flow in microchannels. Int. J. Heat Mass Transfer 40 (13) (1997) 3079-3088

[21] Jain A., Jensen M. K., Analytical modeling of electrokinetic effects on flow and heat transfer in microchannels, International Journal of Heat and Mass Transfer 50 (2007) 5161-5167

[22] Ngoma G., Erchiqui D. F., Heat flux and slip effects on liquid flow in a microchannel, International Journal of Thermal Sciences 46 (2007) 1076–1083

[23] Yıldırım S., Exact and Numerical Solutions of Poisson Equation for Electrostatic Potential Problems, Mathematical Problems in Engineering 2008

[24] Shamshiri M. et al., Heat transfer and entropy generation analyses associated with mixed electrokinetically induced and pressure-driven power-law microflows, Energy 2012

[25] Wang Z., Jian Y., Heat Transport of Electrokinetic Flow in Slit Soft Nanochannels, Micromachines 2019

[26] Jing D. et al., Joule heating, viscous dissipation and convective heat transfer of pressure-driven flow in a microchannel with surface charge-dependent slip, International Journal of Heat and Mass Transfer 108 (2017) 1305–1313